Hydrocarbons in the atmospheric gas phase of a coastal city in Tunisia: Levels, gas–particle partitioning, and health risk assessment

Badreddine Barhoumi, Catherine Guigue, Soufiane Touil, Boris Johnson-Restrepo, Mohamed Ridha Driss, Marc Tedetti

Hydrocarbons in the atmospheric gas phase of a coastal city in Tunisia: levels, gas–particle partitioning, and health risk assessment

Badreddine Barhoumi[a, b, *], Catherine Guigue[b], Soufiane Touil[a], Boris Johnson-Restrepo[c], Mohamed Ridha Driss[a], Marc Tedetti[b,]

[a]*Laboratory of Hetero-Organic Compounds and Nanostructured Materials (LR18ES11), Department of Chemistry, Faculty of Sciences of Bizerte, University of Carthage, 7021 Zarzouna, Tunisia*

[b]*Aix Marseille Univ., Université de Toulon, CNRS, IRD, MIO UM 110, 13288 Marseille, France*

[c]*Environmental Chemistry Research Group, School of Exact and Natural Sciences, University Campus of San Pablo, University of Cartagena, Zaragocilla, Carrera 50 No. 24–99, Cartagena, 130015, Colombia*

*Corresponding authors

E-mail: barhoumibadredine@yahoo.fr

Abstract

Many studies have focused on aliphatic hydrocarbons and polycyclic aromatic hydrocarbons (AHs and PAHs) in different environmental compartments, especially atmospheric particles (aerosols), due to their adverse effects on the environment and human health. However, much less information is currently available on the content of AHs and PAHs in the atmospheric gas phase, which is a major reservoir of volatile and photoreactive compounds. Here, for the first time, we assessed the levels, gas–particle partitioning, human health risks and seasonal variations of AHs and PAHs in the atmospheric gas-phase of Bizerte city (Tunisia, North Africa) over a one-year period (March 2015–January 2016). Σ_{34}PAH concentration in the gas phase over the period ranged from 6.7 to 90.6 ng m^{-3} and on average was 2.5 times higher in the cold season than in the warm season. Σ_{28}AH concentration in the gas phase over the period ranged from 14.0 to 35.9 ng m^{-3}, with no clear seasonal variations. In the gas phase, hydrocarbons were dominated by low-molecular-weight (LMW) compounds, i.e. 3- and 4-ring for PAHs and < *n*-C_{24} for AHs. Gas-phase concentrations of PAHs and AHs accounted for up to 80% of the total (gas + particle phases) atmospheric concentrations of PAHs and AHs. Further analysis of gas–particle partitioning showed that LMW hydrocarbons preferential accumulated in the gas phase, and that gas–particle partitioning was not in equilibrium but dominated by absorption processes into the aerosol organic matter. Benzo[a]pyrene toxic equivalency quotient (BaP-TEQ) in the gas phase represented on average 37% of the total atmospheric BaP-TEQ concentration, which was always higher in the cold season. Atmospheric gas is a significant factor in the risks of cancer associated with inhalation of ambient air. The Monte Carlo simulation-based exposure assessment model predicted that outdoor air exposure to PAHs does not pose a cancer risk to infants, but the children, adolescent, and adult populations may face a lower cancer risk during the warm season and a higher risk in the cold season.

Keywords: Atmospheric pollution; Gas phase; Hydrocarbons; North Africa; Gas–particle partitioning; Health risk

1. Introduction

Among the myriad chemicals dispersed in ambient air, hydrocarbons, chiefly aliphatic hydrocarbons (AHs) and polycyclic aromatic hydrocarbons (PAHs), have been intensively investigated due to their carcinogenic, mutagenic and teratogenic potential (Boström et al., 2002; Weinstein et al., 2010; Honda and Suzuki, 2020). PAHs and AHs are emitted into the atmosphere by human-driven activities such as the exploitation/use of fossil fuels, biomass burning and waste incineration (PAHs), but also from natural sources such as volcanic activity, wildfires (PAHs), and erosion debris from continental higher plants (AHs) (Schauer et al., 2001; Boström et al., 2002; Simoneit, 2002; Ravindra et al., 2008; Yadav et al., 2013).

The transport, deposition, and chemical transformation of PAHs and AHs in the atmosphere are driven by their gas–particle partitioning (Gong et al., 2011; Wang et al., 2011). Like other semi-volatile organic compounds (SVOCs), individual AHs and PAHs are partitioned between particle and gas phases based mainly on their molecular weight, volatility and solubility (Donahue et al., 2012; Pandis et al., 2013). However, their gas–particle partitioning also depends on the environmental factors and climate conditions, including temperature, humidity, precipitation, and windspeed (Munyeza et al., 2019). Consequently, the low-molecular-weight (LMW) PAHs and AHs tend to carry into the gas phase, whereas high-molecular-weight (HMW) hydrocarbons are mainly associated with particulates (Bi et al., 2005; Cincinelli et al., 2007). This makes it important to consider both the gas and particle phases, which span a size continuum and encompass a complementary spectrum of compounds, when investigating hydrocarbon atmospheric pollution.

The majority of studies dealing with PAHs/AHs in the atmosphere focus only on the particle phase (aerosols). This is because most of the known toxic hydrocarbons are HMW and low-volatility compounds that preferentially carry into primary organic aerosols (POAs) when they are freshly emitted (Tomaz et al., 2016). However, several recent observations

underline the importance of gas-phase matter. 1) It is the smallest atmospheric material (< 1 µm), thought to have the most harmful effects on human health (Andersen et al., 2010; Belleudi et al., 2010; Liu et al., 2013; Meng et al., 2013; Lin et al., 2016). This material can penetrate *via* inhalation into the lungs and reach the bloodstream, causing adverse effects (Valavanidis et al., 2008; Manisalidis al., 2020). 2) SVOCs in the gas phase serve as precursors to secondary organic aerosols (SOAs) due to atmospheric photochemical aging (de Gouw et al., 2011; Shi et al., 2019a, b). SOAs are thought to have a radically different impact on human health and climate compared primary emissions that have a far lower degree of oxidation than SOAs (Robinson et al., 2007). 3) Photoproducts from photooxidation processes occurring in the gas phase may be much more toxic than their parent compounds (Tomaz et al., 2016; Mulder et al., 2019). 4) Through air–water exchanges, PAHs present in the gas phase are a significant source of dissolved PAHs in the marine environment that can then enter marine trophic chains and disrupt biogeochemical cycles and ecosystem functioning (Dachs and Méjanelle, 2010; Duran and Cravo-Laureau, 2016; González-Gaya et al., 2019).

Despite the deterioration of air quality in Africa due to population growth, urbanization, traffic emissions, open burning and the transport of Saharan dust, there are still limited studies available on atmospheric hydrocarbon levels, especially in the gas phase (Fayiga et al., 2018; Munyeza et al., 2019). Barhoumi et al. (2018) reported AH and PAH levels in total aerosols and hydrocarbon risk assessment data in Bizerte city (Tunisia, North Africa). Here, to gain a deeper understanding the atmospheric hydrocarbon load in this area, we performed this study to investigate AHs and PAHs in the atmospheric gas phase over Bizerte city during one year (March 2015–January 2016), with a focus on the levels, gas–particle partitioning and human health risks of AHs and PAHs, and their seasonal variations.

2. Materials and methods

2.1. Study site and sampling

Sampling was carried out on the roof of the Faculty of Science of Bizerte in the 'Zarzouna' district (37° 16' 0.5802" N, 9° 52' 49.875" E), approximately 1 km from Bizerte city center (Tunisia, North Africa; see Fig. S1 in Supplementary information (SI)). Further description of the study site and sampling procedures are reported in previous work (Barhoumi et al., 2018, 2020 a,b). Briefly, Bizerte is a medium-size city (~127,000 inhabitants), with economic activity focused mainly on fishing, agriculture, and light and heavy industry including a cement factory located north-west of the sampling site, a petroleum refinery, the Tunisian Company of Lubricants (SOTULUB), and other mechanics, electronics, plastics, and textiles industries located south-east of the sampling site. In addition to these activities, there is substantial anthropogenic pressure driven by the high traffic density (public transport, touristic and merchant shipping) and strong urbanization. Bizerte city has a predominantly humid climate (average relative humidity is around 70%), and weather conditions are usually hot in summer and mild in spring, with annual precipitation rates varying between 300 and 800 mm (mainly concentrated in the fall and winter months), and frequent northwest winds (200 days per year, with an average windspeed of 6-8 m s^{-1}; Castro Jiménez et al., 2017).

Sampling was conducted with a high-volume air sampler (HVAS, Tisch Environmental Inc., OH) equipped with pre-weighed, pre-combusted quartz fiber filters (QFF, 20.3 × 25.4 cm, Whatman QMA-grade) to collect the particle (aerosol) phase samples, and pre-cleaned polyurethane foams (PUF; 7.6 × 7.6 cm, Tisch Environmental TE-1123-6) to collect gas phase samples. The HVAS, which was calibrated before being used according to the manufacturer's instructions, was operated at an average flowrate of 0.66 m^3 min^{-1} for 48 h from March 2015 to January 2016 (n=53). Data on the particle-phase measurements has already been published (Barhoumi et al., 2018). Prior to sampling, the PUFs were pre-cleaned

with dichloromethane (DCM) using pressurized solvent extraction (ASE 350, DIONEX; three DCM cycles of 10 min: 100°C, 110 bars, 100% rinsing volume, 60 s purging time). After sampling, the load-carrying PUFs were individually wrapped in double pre-combusted aluminium foils, sealed in polyethylene bags, and immediately transported to the laboratory where they were stored frozen at -20°C. Field blanks were generated every month by placing PUFs in the HVAS for a few seconds without switching it on. Details on sampling dates, sampling duration and collected air volumes are reported in SI (Table S1), along with total suspended particle (TSP) concentrations for each sample. Meteorological parameters including wind speed and direction, relative humidity, ambient temperature and rainfall were provided by the National Institute of Meteorology located near the sampling station.

2.2. Sample processing and analysis

In this work, we determined 28 AHs (26 resolved long-chain *n*-alkanes, i.e. *n*-C_{15} to *n*-C_{40} and the two isoprenoids phytane (Phy) and pristane (Pr), the unresolved complex mixture (UCM), which corresponds to aliphatic branched and cyclic hydrocarbons that are not separable as individual compounds), 19 parent PAHs, and 15 alkylated PAHs. The parent PAHs included naphthalene (Nap), acenaphthylene (Acy), acenaphtene (Ace), fluorene (Fl), dibenzothiophene (DBT), phenanthrene (Phe), anthracene (Ant), fluoranthene (Flu), pyrene (Pyr), benz[*a*]anthracene (BaA), chrysene (Chr), benzo[*b*]fluoranthene (BbF), benzo[*k*]fluoranthene (BkF), benzo[*e*]pyrene (BeP), benzo[*a*]pyrene (BaP), perylene (Per), dibenz[*a,h*]anthracene (DahA), benzo[*g,h,i*]perylene (BghiP), and indeno[1,2,3-*cd*]pyrene (IcdP). The alkylated PAHs were the methyl-, dimethyl-, trimethyl- homologs (C1-, C2-, C3-, respectively) of the five target compounds Nap, Fl, Phe, Pyr and Chr. We used the alkylated PAHs/parent compounds (Alk/Par) ratio as an index of PAH sources, as a predominance of alkylated compounds points to petrogenic inputs (Azimi et al., 2005). PUF samples were spiked with 100 µL mixtures of deuterated standards (surrogates): Nap-d_8, Fl-d_{10}, Phe-d_{10},

Flu-d_{10} and BaP-d_{12} for PAHs (2 mg L^{-1} each), and C_{16}-d_{34}, C_{24}-d_{50} and C_{36}-d_{74} for AHs (20 mg L^{-1} each), then extracted with DCM using ASE. The extracts were concentrated using a rotary evaporator, then solvent-exchanged by *n*-hexane to ≈ 200 µL, and cleaned with a silica-alumina column (10 mm i.d., made of glass) packed from bottom to top with 3 g deactivated alumina (with 3% water w/w), 3 g activated silica, and 1 g dehydrated sodium sulfate. AHs and PAHs were co-eluted with 50 mL of *n*-hexane/DCM (80:20 v/v), followed by a pre-analysis solvent reduction and added with a mixture of deuterated (internal) standards: Ace-d_{10}, Ant-d_{10}, Pyr-d_{10}, Chr-d_{12} and Per-d_{12} for PAHs, and C_{19}-d_{40} and C_{30}-d_{62} for AHs.

Cleaned extracts were analyzed by gas chromatography (Trace ISQ, Thermo Electron) equipped with a mass spectroscopy detector with hydrogen (1.2 mL min^{-1}) as carrier gas. Injection volume was 1 µL. The capillary column (HP-5MS, Agilent Technologies, USA) was 30 m in length with an internal diameter of 0.25 mm and a film thickness of 0.25 µm. The injector temperature (used in splitless mode) was 250°C and detector temperature was 320°C. Column temperature was first held at 70°C for 3 min, then ramped to 150°C at 15°C min^{-1}, ramped to 320°C at 7°C min^{-1}, and held for 10 min. Mass spectrometry (MS) was operated in electron impact (EI) mode (70 eV), and PAHs and AHs were identified and quantified in full scan and selected ion monitoring (SIM) modes simultaneously, using two distinct methods (Guigue et al., 2011, 2014, 2017). Quantification was carried out using internal standards, and sample concentrations are expressed in ng m^{-3}. All solvents (Rathburn Chemicals Ltd, Scotland) were HPLC-grade. Standards were ≥ 98% purity-grade and clean-up powders were high-purity grade (Merck, Sigma Aldrich, France).

2.3. Quality assurance and quality control (QA/QC)

The QA/QC procedures were strictly followed throughout the whole sampling and laboratory treatment process. QA/QC included control/validation of GC/MS calibration and tuning, laboratory and field blanks, method detection limit (MDL), and surrogate recoveries.

Field and laboratory blanks were prepared, processed and analyzed in the same manner as the real samples. The results showed that only trace levels of LMW PAHs (Nap and C1-Nap) and AHs (*n*-C_{15}–*n*-C_{20}, Pr and Phy) were detected in the field blanks. Concentrations of these compounds in the blanks represented less than 7% of the concentrations found in the real samples. PUF sample concentrations were corrected for the corresponding average field blank. MDLs, which were calculated from signal-to-noise ratios of 3 (considering an average sampled air volume of 1920 m^3), ranged from 0.3 to 3 pg m^{-3} for PAHs, and from 3 to 10 pg m^{-3} for AHs (Table S2). Compounds with concentrations below the MDL were considered as not detected in the sample, and thus assumed to be zero in the statistical analyses. For PAHs, surrogate recovery rates were 69% for Nap-d_8, 76% for Fl-d_{10}, 95% for Phe-d_{10}, 82% for Flu-d_{10} and 100% for BaP-d_{12}. For AHs, surrogate recovery rates were 75% for C_{16}-d_{34}, 103% for C_{24}-d_{50} and 88% for C_{36}-d_{74}. All data reported here has not been corrected for recoveries.

2.4. Data handling

To describe the partitioning behavior of PAHs and AHs, we calculated the gas–particle (G/P) partitioning coefficient, K_p (m^3 μg^{-1}), as follows:

$$K_P = \frac{C_P / TSP}{C_g} \qquad (1)$$

where C_p and C_g are the PAH and AH concentrations in the particle and gas phases, respectively (ng m^{-3}), and TSP is the concentration of total suspended particles in the air (µg m^{-3}) (Pankow, 1994a**;** Terzi and Samara, 2004). Concentrations of PAHs and AHs in the particle phase were obtained from Barhoumi et al. (2018). Multiplying K_p by TSP gives the ratio between the concentrations in the particle and gas phases:

$$K_P \times TSP = C_P / C_g \qquad (2)$$

If K_p × TSP value is < 1, then that compound partitions primarily into the gas phase, whereas if *K*p × TSP is > 1, then that compound partitions primarily into the particle phase (Volckens and Leith, 2003).

The G/P partitioning of SVOCs in the atmosphere can generally be explained by two different mechanisms: adsorption onto the aerosol surface, and absorption into organic matter (Pankow, 1994a). Both mechanisms lead to a linear relationship between log K_p and log supercooled vapor pressure, P_L^0, which is expressed as (Caliskan et al., 2020):

$$\log K_P = m_r \log P_L^0 + b_r \qquad (3)$$

where m_r, the slope, and b_r, the intercept of the regression, are empirical constants. Log K_p was regressed on $\log P_L^0$ for each sampling event (n = 53) to determine m_r and b_r. Only those PAHs and AHs found at concentrations above the MDLs (in both phases) for a given sample/event were used in the regression of log K_p *vs* $\log P_L^0$. In theory, where there are no experimental errors and interferences, slope values (m_r) should be close to -1 under equilibrium conditions. If m_r is higher than -1, then adsorption (onto the aerosol surface) is the dominant mechanism. If m_r is lower than -0.6, then absorption (into organic matter) is the dominant mechanism. If m_r is between -1 and -0.6, then both adsorption and absorption are at work (Pankow, 1994a, b**;** Terzi and Samara, 2004).

The temperature-dependent P_L^0 of PAHs and AHs was calculated using the following equation:

$$\log(P_L^0, Pa) = m_L / T + b_L \qquad (4)$$

where T is daily average temperature (K) during each sampling event, and m_L and b_L are regression parameters specific to each compound, as reported by Lei et al. (2002) and Vuong et al. (2022). Table S3 gives the m_L and b_L values of selected compounds. For compounds for which no m_L and b_L values were available, the $\log P_L^0$ values were estimated using the following equation (Xie et al., 2014):

$$P_L^0 = P_L^{0,*} * \exp[\frac{\triangle H_{vap}^0}{R}\left(\frac{1}{298.15} - \frac{1}{T}\right)] \qquad (5)$$

where $P_L^{0,*}$ is the subcooled vapor pressure of each compound at 298.15 K obtained from EPI Suite version 4.11 (*http://www.epa.gov/opptintr/exposure/pubs/episuitedl.htm*), ΔH_{vap}^0 is the enthalpy of vaporization at standard conditions (kJ mol^{-1})) of each compound at 298.15 K obtained from the *https://www.chemeo.com/* database (Table S3), and R is the gas constant (8.314 J mol^{-1} K^{-1}).

When absorption into organic matter was the dominant process, the temperature-dependent octanol-air partitioning coefficient, K_{OA}, was used with success as an alternative to P_L^0 to describe G/P partitioning (Harner and Bidleman, 1998**;** Esen et al., 2006**;** Wang et al., 2013). The relationship between log K_p and log K_{OA} is defined by the following equation, with equilibrium partitioning *n* being expected to have a value of +1:

$$\log K_P = n \log K_{OA} + c \qquad (6)$$

where the slope *n* and intercept of the regression *c* are empirical constants, and log K_{OA} calculated from the following equation using temperature (in K) and available literature values for A and B (Parnis et al., 2015**;** Vuong et al., 2022) (Table S3):

$$\log K_{OA} = A + B/T \qquad (7)$$

2.5. Health-risk assessment

The benzo[*a*]pyrene toxic equivalency (BaP-TEQ) was used as an indicator to assess the health risks associated with exposure to in-air PAH (WHO, 1987**;** Bandowe et al., 2014), and is estimated as follows:

$$\mathrm{BaP-TEQ} = \sum_{i=1}^{n}(\mathrm{PAHi} \times \mathrm{TEFi}) \qquad (8)$$

where the index *i* runs over the *n* PAHs (here, *n*=16 (EPA priority PAHs) or 22 (all PAHs presenting a toxic equivalency factor (TEF)); see Table S4), PAHi is the individual concentration of each PAH (ng m^{-3}), and TEFi is the corresponding TEF for each PAH. Here,

for most of the PAHs, we were able to use the TEF proposed by Nisbet and LaGoy (1992). For PAHs with no known TEF (BeP, Per, C1-Nap, C1-Phe, and C1-Pyr), we used values suggested by other studies (Durant et al., 1996; Hsu et al., 2014; CalEPA, 2020). Table S4 reports the list of TEFs adopted in this study.

Furthermore, we used the incremental lifetime cancer risk (ILCR) method to quantitatively assess the risk of PAHs exposure through inhalation based on the US EPA reference model (US EPA, 2005; Peng et al., 2011). Here, ILCR was determined for four age groups: infants (0–1 years old), children (1–11 years old), adolescents (12–17 years old), and adults (18-30 years old). The computational formula used for ILCR, calculated here for the gas and particle phases, is as follows:

$$ILCR_{inhalation} = CSF_{inhalation} \times \frac{C \times IR_{inhalation} \times EF \times ED \times C_f}{BW \times ALT} \quad (9)$$

where C (ng m^{-3}) is total (gas + particle) BaP-TEQ concentration, $IR_{inhalation}$ (m^3 day^{-1}) is inhalation rate, EF (days $year^{-1}$) is exposure frequency, ED (year) is exposure duration, C_f is the ng-to-mg conversion factor (10^{-6}), BW (kg) is body weight, ALT (year) is average life span, and $CSF_{inhalation}$ ((mg kg^{-1} day^{-1})$^{-1}$) is the cancer slope factor, which assumed to be 3.14 ± 1.80 (mg kg^{-1} day^{-1})$^{-1}$ (Chen and Liao, 2006). Table S5 gives details of the parameters used to estimate ILCR values for the different age-groups.

Monte Carlo simulation generates a large number of random samples or scenarios and then use these to estimate the probability distribution of the ILCR or the outcomes of interest. In this case, the outcomes of interest are the probabilities of developing cancer from exposure to PAHs. The carcinogenic risk assessment was conducted for exposure to PAHs through air inhalation by using Monte Carlo simulation with the Crystal Ball software, version 11.1.2.4 (Oracle, Inc., Redwood, USA). A comprehensive explanation of abbreviations, probability distribution, and units for the input parameters such as $IR_{inhalation}$, C, EF, ED, BW, ALT, and

$CSF_{inhalation}$ can be found in Table S5. To ensure accuracy and uncertainty analyses, 10,000 random repetitions for all calculations were performed for the estimation of the ILCR.

2.6. Statistical analysis

All statistical analysis was performed using SPSS software (version 20.0) and XLSTAT (version 2021.1.1). Student's parametric *t*-test was used to determine significant differences between group means related to season (warm *versus* cold seasons), with each group including between 17 and 36 samples. Comparisons were performed using the non-parametric Mann–Whitney test, which gave the same results as the *t*-test in terms of significant/non-significant differences, with significance level set at $p < 0.05$. Figures were plotted using GraphPad Prism 5 software, and calculations were performed using Microsoft Excel 2016.

3. Results and discussion

3.1. Concentrations and molecular profiles

To investigate the seasonal variations of PAH and AH distributions (concentrations and molecular profiles) in the atmospheric gas phase, the year was divided into two periods defined as warm season (spring–summer, from March to August 2015, n=36) and cold season (fall–winter, from September 2015 to January 2016, n=17) based on prevailing meteorological conditions in Bizerte city (Barhoumi et al., 2018). Ambient temperature (AT), wind speed (U), wind direction (WD), relative humidity (RH), and other meteorological parameters can significantly influence atmospheric pollutant loading (Chirico et al., 2007**;** Elorduy et al., 2016). Here, during the warm and cold seasons, AT was 21.4 ± 5.7°C and 18.3 ± 5.9°C, RH was 68.1 ± 6.6% and 73.9 ± 9.7%, U was 4.4 ± 1.7 and 3.3 ± 1.9 m s^{-1}, and precipitation was 0.2 ± 0.8 and 0.3 ± 0.5 mm, on average, respectively (Table S1).

Σ_{34}PAH concentration in the gas phase during the study period ranged from 6.7 to 90.6 ng m^{-3} with an annual mean of 20.4 ± 17.2 ng m^{-3} (Table 1; Fig. 1a). These concentrations were of the same order of magnitude as those recorded in atmospheric gas-phase analyses in Prato (Italy), Athens and the island of Crete (Greece) (Cincinelli et al., 2007; Vasilakos et al., 2007; Iakovides et al., 2021) but much lower than those recorded in West-African port cities (Munyeza et al., 2019). Note, however, that it is difficult to reliably compare data obtained by different research groups, as the geological characteristics of the sampling areas, the number of samples taken, and the number of PAHs analyzed may not be the same. Gas-phase PAH concentrations showed seasonal variations. Σ_{34}PAH concentration averaged 13.8 ± 6.6 ng m^{-3} and 34.4 ± 23.7 ng m^{-3} during the warm and cold seasons, respectively (Table 1; Fig. 1a). Σ_{34}PAH concentrations were on average 2.5-times higher in the colder months than in the warmer months (*t*-test, $p<0.0001$). This seasonal trend, i.e. higher levels in the colder season, is in line with previous work (Vasilakos et al., 2007; Hassan and Khoder, 2012; Caliskan et al., 2020). In addition, Alk/Par ratio was significantly higher during the warm season (2.3 ± 0.7) than in the cold season (1.8 ± 0.7) (*t*-test, $p<0.0001$). This PAH compound ratio has been used previously to help determine the origin of hydrocarbon contamination and identify the major weathering processes. Crude oils and many refined petroleum products have a higher ratio of alkylated PAHs to parent PAHs than engine exhaust emissions that have a lower ratio due to thermal dealkylation within the engine (Schauer et al., 1999). Biomass burning has also shown low Alk/Par ratios (Schauer et al., 2001). Moreover, Alk/Par ratio would increase with photodegradation, because the alkyl derivatives show lower photodegradation rates than the parent compounds (García-Martínez et al., 2006). Thus, these seasonal trends in both PAH concentrations and Alk/Par ratio would mainly be due to 1) increased usage of fossil fuels/biomass burning, especially for heating, combined with specific atmospheric conditions in winter (Bamford and Baker, 2003; Reisen and Arey, 2005; Manoli et al., 2016) and 2) the

photolytic and thermal decomposition of PAHs in summer (Albinet et al., 2007; Cincinelli et al., 2007; Sharma et al., 2007). Finally, the AT, RH, Σ_{34}PAHs and Alk/Par parameters all correlated well together (Pearson's correlations, r=-0.59–0.55, n=53, p<0.0001-0.044; data not shown), which clearly illustrates the seasonality of gas-phase PAH loading.

During the study period, the Σ_{34}PAH concentration recorded in the gas phase represented on average 89 ± 5.1% of the total (gas + particle phases) Σ_{34}PAH concentration (Fig. 1a) (Barhoumi et al., 2018). This trend was consistent with previous studies reporting higher levels of gas PAHs relative to particle-bound PAHs (Terzi and Samara, 2004; Abdallah and Atia, 2014; Ishtiaq et al., 2021). Furthermore, molecular distribution data showed that gas-phase PAHs were dominated by 3-ring compounds (76% of Σ_{34}PAHs on average during the study period), chiefly Phe (22%), C1-Phe/Ant (20%) and C2-Phe/Ant (11%) (Fig. 1b), as already observed by Tsapakis and Stephanou (2005). The molecular distribution profiles were completed by 4-ring compounds (19%) and 2-ring compounds (4.6%), with a very minor contribution from 5- and 6-ring compounds (~0.1%) (Fig. 1b). Hence, the LMW (2-4 rings) PAHs accounted on average for 80.3%–98.8% of the gas-phase load, whereas the HMW (5-6 rings) PAHs accounted for 96.7%–99.4% in the particle-phase load (Fig. 1b, c). These results are in good agreement with the fact that the LMW-PAHs have high vapor pressures and low octanol-air partition coefficients and are generally found in the gas phase, whereas the reverse is true for the HMW-PAHs, which are usually attached to the particle phase, have low vapor pressures and high octanol-air partition coefficients (Terzi and Samara, 2004; Ma et al., 2019). Below we examine the gas–phase partitioning of hydrocarbons in greater depth.

Σ_{28}AH concentration in the gas phase during the study period ranged from 14.0 to 35.9 ng m^{-3} with an annual mean of 22.5 ± 5.3 ng m^{-3} (Table 2; Fig. 2a). Contrary to PAHs, Σ_{28}AH no did not show any clear variation between the warm-season (22.0 ± 4.8 ng m^{-3}) and cold-season periods (23.7 ± 6.1 ng m^{-3}) (Table 2; Fig. 2a). In addition to resolved compounds, we

also recorded UCM structures in the AH analyses. The annual mean concentration of UCM was estimated at 90.7 ± 30.9 ng m^{-3}, with 90.4 ± 33.6 ng m^{-3} for the warm season and 91.3 ± 26.2 ng m^{-3} during the cold season, and an average UCM/R ratio of 4.1.

During the study period, the Σ_{28}AH concentration recorded in the gas phase represented on average 47% of the total (gas + particle) Σ_{28}AH concentration (Fig. 2a). Nevertheless, this percentage increased up to 80% when taking the UCM into account. Figs. 2b and 2c show that *n*-C_{17}-*n*-C_{24} compounds were mainly found in the gas phase while > *n*-C_{24} compounds were mostly found in the particle phase. In the gas phase, the resolved compounds displayed a monomodal molecular distribution centred on *n*-C_{22} (18%), without any dominance of odd- or even-numbered *n*-carbon compounds (Fig. 2b). This points to an anthropogenic (petrogenic) origin of AHs in the gas phase. In addition, Σ_{28}AH concentration was slightly but significantly positively correlated to UCM and Σ_{34}PAH concentrations in the gas phase (Pearson's correlation, r=~0.37, n=53, p=0.005–0.008; data not shown). This observation, in agreement with previous studies, reinforces the assumption of petrogenic-origin AHs through fossil fuel emissions (Schauer et al., 1999, 2002; Mandalakis et al., 2002; Cincinelli et al., 2007), although biomass burning may also contribute to the AH signature in the gas phase (Schauer et al., 2001).

Surprisingly, compared to known oil fingerprints, the lowest-molecular-weight compounds (2-ring PAHs with alkylated homologs and < *n*-C_{19} AHs) were relatively unabundant in the gas phase (Wang et al., 1999). One explanation could be the fact that LMW PAHs and AHs in the gas phase, which have been identified as important SOA contributors in urban areas (Robinson et al., 2007; de Gouw et al. 2011; Yuan et al., 2013; Zhao et al., 2014; Li et al., 2022) especially due to vehicle emissions (Yuan et al., 2013; Zhao et al., 2015; Liggio et al., 2016; Ding et al., 2017; Liu et al., 2017; Luo et al., 2019), undergo transformation by chemical reactions with hydroxyl radicals (OH), chlorine atoms (Cl), nitrate radicals (NO_3) or

ozone (O_3) (Atkinson, 2000). We also cannot rule out that the relative lack of LMW compounds in the gas phase may come from a sampling bias. Indeed, some authors have underlined that because Naph, Acy and Ace PAHs and < *n*-C_{19} AHs possess relatively high vapor pressures, they may not be efficiently trapped by this method used (Jolley and Wang, 1992). However, the PAH and AH compounds recorded here in the gas phase already represented more than 80% of the ambient air loading, either in terms of mass concentrations or in terms of pool of reactants/precursors for harmful material.

3.2. Gas–particle partitioning

3.2.1. Gas–particle phase concentrations

Understanding the phase distribution of PAHs and AHs in atmosphere is important for evaluating their fate, transport, transformation, and potential environmental/health impacts (Simcik et al., 1998**;** Gaga and Ari, 2019**;** Ma et al., 2019). Here we computed the G/P partitioning coefficient (log K_p) and K_p × TSP of each PAH and AH using Eq. (1) and Eq. (2). The average, minimum, median and maximum values of K_p × TSP and log K_p are summarized in Table S6. The median values of K_p × TSP for individual PAHs (up to BaA/Chr, MW ~228-230) and AHs (up to *n*-C_{24}, MW ~338) were < 1, which explain their preferential accumulation in the gas phase. This is consistent with results reported above and in Figs. 1c and 2c, which show the dominance of LMW PAHs and AHs in the gas phase and of HMW PAHs and AHs in the particle phase. The mean log K_p for individual PAHs and AHs ranged from -3.63 (DBT) to -0.042 (BghiP) and from -3.06 (*n*-C_{16}) to -0.305 (*n*-C_{30}), respectively (Table S6). The log K_p values for PAHs were in good agreement with values previously determined in Finokalia, Greece (-3.83 < log K_p < -0.66) (Tsapakis and Stephanou, 2005). Except for LMW compounds, i.e. PAHs of MW < 166–170 and AHs < *n*-C_{19}, the log K_p values increased with molecular weight of the compounds. This trend has already been found in previous studies (Cincinelli et al., 2007**;** Cao et al., 2018). We can therefore conclude that

the difference in log K_p among the different PAHs and AHs is mainly related to their different physical-chemical properties.

3.2.2. Sorption mechanisms

Adsorption onto the aerosol surface and absorption into the aerosol organic matter are two different mechanisms that have been used to describe the G/P partitioning of SVOCs (Pankow, 1994a). The linear relationships between log K_p and log P_L^0 (Eq. 3) can describe these two mechanisms and thus afford useful information (extracted from the empirical constants m_r and b_r) about the partitioning of the compounds. Figs. 3a and 3c plot these relationships for PAHs and AHs across the whole sampling period. Due to the limited number of the lowest-MW compounds (although plotted on figures in red), we did not include these lowest-MW compounds in the calculation of the regression parameters. Both compound classes showed good linear relationships, with r values of -0.92 (PAHs) and -0.88 (AHs). The m_r slope values were -0.71 for PAHs and -0.46 for AHs. Similarly, the intercept b_r, which is mainly related to the physical properties of aerosols, was -4.40 for PAHs and -3.6 for AHs (Figs. 3a and 3c). These values were within the range of data reported in the literature (Table S7). The slopes obtained were lower than the expected slope under equilibrium conditions (-1.0), but this deviation does not necessarily indicate disequilibrium, as certain factors can cause the slopes m_r to deviate from -1 (Goss and Schwarzenbach, 1998; Simcik et al., 1998). Sampling artefacts, such as absorption of gas-phase compounds onto the quartz filters, presence of nonexchangeable compounds on atmospheric particles, non-equilibrium conditions due to the closeness of the sources to the sampling point, chemical and physical characteristics of TSP, meteorological conditions, and a lack of constancy in activity coefficients, might be the main reasons for slope-values deviations from -1 (Goss and Schwarzenbach, 1998; Dachs and Eisenreich, 2000; Vardar et al., 2004; Su et al., 2006; Akyüz and Çabuk, 2010). BaP-to-BeP ratio has been used as indicator of long-range transport

(Kim et al., 2012), and the fact that it did not significantly correlate with m_r ($r = 0.05$, $p > 0.05$) may point to dominant local emission sources in this area. Indeed, previous research in this area has already suggested a dominance of local-source factors (vehicle exhaust, Bizerte harbor, the cement factory, the Zarzouna petroleum refinery, the Tunisian Company of Lubricants, Menzel Jemil electronics, plastics and textile industries) relative to meteorological conditions (Barhoumi et al., 2018).

The K_{OA} value can also be used as an alternative to P_L^0 to describe the G/P partitioning. Here we found A strong positive correlation between the measured log K_p and log K_{OA} for PAHs ($r = 0.91$, $p < 0.0001$) (Fig. 3b). The slope *n* was 0.60, thus lower than the value of the partitioning equilibrium (1.0), which also indicates that PAHs had not reached equilibrium between the gas and particle phases. The slope *n* was much steeper than the slope m_r from log K_p vs $\log P_L^0$, thus confirming that absorption was the dominant sorption mechanism in studied area. The slope *n* value found here was similar to the value reported for an urban site in Beijing, China ($n = 0.63$; Ma et al., 2011).

3.3. Health-risk assessment

The annual trend of BaP-TEQ concentrations for both gas and particle phases of 22 PAHs is depicted in Fig. 4a. The mean BaP-TEQ (gas + particle) concentration for the whole study period was 0.25 ± 0.31 ng m^{-3} and was 3 times higher in the cold season (mean of 0.45 ± 0.48 ng m^{-3}) than in the warm-season period (mean of 0.16 ± 0.11 ng m^{-3}). Two values, i.e. 1.4 on 18 December 2015 and 1.8 ng m^{-3} on 25 December 2015, were above the WHO reference threshold (1 ng m^{-3}). During the study period, the gas-phase BaP-TEQ concentration from the represented on average 37% ± 15% of the total (gas + particle phases) BaP-TEQ concentration (Fig. 4b). Interestingly, among all TEF-PAH members (PAHs associated with TEF factors; see Table S4) included in the BaP-TEQ calculation, C1-Pyr (84% originating from the gas phase) was the most important carcinogenic contributor at 29.1% of total BaP-

TEQ, more than BaP (23.6%) and DahA (12.7%) (Fig. S2a). Note that C1-Pyr does not belong to the 16 USEPA-listed PAHs, and thus this shows that the impact of the non-USEPA-listed PAHs to total PAH toxicity is significant and should not be overlooked (Fig. S2a, b). It is vital to consider this contribution of the gas phase to the total BaP-TEQ concentration, as we assume that an important fraction of the LMW compounds were either not trapped in the PUF or were phototransformed into by-products that are even more toxic than their parents or that drive SOA formation. These results further argue for a potential role of the gas phase and support the fact efforts to better understand and estimate the toxicity of the atmosphere needs to focus on contaminant distribution and dynamics in all compartments. The gas phase can be inhaled more easily and transported across the lungs into the bloodstream (Ramírez et al., 2011), and had already been found to be a bigger driver of cancer risk than particulates (Hassan and Khoder, 2012**;** Tomaz et al., 2016).

The estimation of ILCR (using Eq. 10 and the mean values of the parameters presented in Table S5) is another way to estimate the cancer risk incurred from exposure to PAHs (from gas + particle phases) *via* inhalation from outdoor sources. An ILCR of $< 10^{-6}$ is classified as very low potential risk, an ILCR between 10^{-6} and 10^{-4} is classified as low potential risk, an ILCR between 10^{-4} and 10^{-3} is moderate, and an ILCR $\geq 10^{-3}$ denotes a high potential health risk (Caliskan et al., 2020). Table 3 lists the estimated ILCR values for each specific age-group for cold and warm season as well as over the whole year. The ILCR values generally increased with age, from infants (0-1 year) to adults (18-70 years). In contrast, adolescents (12-17 years) have lower ILCR values than children aged 1-11 years. This was mainly attributed to the relatively lower body weight and higher ED values of the children group. The highest ILCR value (5.7×10^{-4}) was found in the adult group (18–70 years), suggesting that adults over 18 years old may be at higher risk of developing cancer due to a longest duration of exposure. The total accumulated ILCR for all the age-specific groups during the whole year

varied from 2.0×10^{-5} to 8.9×10^{-4} (mean of $1.3\times10^{-4} \pm 1.5\times10^{-4}$) and was significantly higher (*t*-test, $p<0.0001$) in the cold season (mean of $2.3\times10^{-4} \pm 2.4\times10^{-4}$) than in the warm season (mean of $8.2\times10^{-5} \pm 5.6\times10^{-5}$). All ILCRs were between 10^{-6} and 10^{-3}, indicating low to moderate risk. Note that ILCR values were calculated based on outdoor sources only. However, the indoor sources may lead to even higher ILCR values due to additional sources such as cooking fumes, tobacco smoke, and residential heating (Ramírez et al., 2011; Shen et al., 2013).

Monte Carlo simulation is a powerful tool used on this study to estimate ILCR by incorporating uncertainty and variability in the input parameters. This approach provided a more realistic and accurate estimate of the risk of developing cancer from exposure to PAHs in outdoor air through inhalation. The Monte Carlo simulation allowed us to calculate the cumulative distribution function (CDF) of the predictive inhalation lifetime cancer risk (ILCR), which was useful for visualizing the data for all age groups experiencing different levels of health risks due to exposure to PAHs in outdoor air. Plotting the CDF of the ILCR for the annual period (Fig. 5), the cancer risk threshold (represented by the red line) indicated that infants faced no health risk. However, the 95% adult population (>5th percentile) had a low potential risk (ranging from $1.1\text{x}10^{-5}$ to $2.6\text{x}10^{-4}$). Additionally, the 50% population (>50th percentile) of children (with risks ranging from $1.7\text{x}10^{-5}$ to $8.2\text{x}10^{-5}$) and adolescents (with risks ranging from $1.1\text{x}10^{-5}$ to $5.2\text{x}10^{-5}$) may also face low potential risks (Table 3). Overall, during the cold season, all age groups experienced higher health risks compared to the warm season (Fig. S3). For the cold season, while the 95% adult population (>5th percentile) may face a low potential risk, 75% of the children and adolescent population (>25th percentile) may also face low potential risks. Infants, on the other hand, may face health risks only if they are part of the 5% of the population (>95th percentile) (Table 3).

4. Conclusions

This study shows that the gas phase carrying LMW compounds (3- and 4-ring PAHs and < *n*-C_{24} AHs) may contribute up to 80% of the total (gas plus particle-borne) hydrocarbon concentration and up to 40% of the total hydrocarbon toxicity (BaP-TEQ concentration) in the atmosphere. If we factor in a possible sampling bias of the PUFs (which do not retain all the LMWs) and the reactivity of the compounds in the gas phase (transformation into photoproducts or secondary organic aerosols), then we can assume that the actual toxicity of the gas phase is even greater. Gas-phase PAH concentrations were higher during the colder season, whereas gas-phase AH concentrations showed no marked seasonal pattern. This work also highlights that atmospheric hydrogen toxicity involves not only the 16 listed PAHs studied but also other (methylated) aromatic compounds, such as C1-Pyr. We conclude that the gas phase is an essential compartment that needs to be addressed to properly investigate the levels, dynamics, chemical/photochemical reactivity, and impact/toxicity of hydrocarbons in the atmosphere. According to the Monte Carlo simulation-based exposure assessment model, outdoor air exposure to PAHs was predicted to not pose a cancer risk to infants. However, the model indicates that children, adolescents, and adults may have a low cancer risk during the warm season and a high risk in the cold season. Future investigations on the gas phase should focus on the reactivity of the compounds and their transformation into secondary organic aerosols, as these secondary aerosols are known to cause impactful adverse effects on both human health and climate.

Data availability

Data will be made available on request.

Declaration of Competing Interest

The authors declare that they have no known competing financial interests or personal relationships that could have appeared to influence the work reported in this paper.

Acknowledgements

This research work was funded by the Institut de Recherche pour le Développement (IRD), through the "COSYS-Med" joint international laboratory ('LMI'), by the Tunisian Ministry of Higher Education and Scientific Research, by the PACA region-sponsored 'Particule' project, and by the IRD-MIO Action Sud 'AEROBIZ' project. We thank two anonymous reviewers and the associate editor for their constructive comments on the manuscript.

Appendix A. Supplementary data

Supplementary data to this article can be found online at https://doi. org/…

References

Abdallah, M.A.-E., Atia, N.N., 2014. Atmospheric concentrations, gaseous–particulate distribution, and carcinogenic potential of polycyclic aromatic hydrocarbons in Assiut, Egypt. Environ. Sci. Pollut. Res. 21, 8059–8069.

Akyüz, M., Çabuk, H., 2010. Gas–particle partitioning and seasonal variation of polycyclic aromatic hydrocarbons in the atmosphere of Zonguldak, Turkey. Sci. Total Environ. 408, 5550–5558.

Albinet, A., Leoz-Garziandia, E., Budzinski, H., ViIlenave, E., 2007. Polycyclic aromatic hydrocarbons (PAHs), nitrated PAHs and oxygenated PAHs in ambient air of the Marseilles area (south of France): concentrations and sources. Sci. Total Environ. 384, 280–292.

Andersen, Z.J., Olsen, T.S., Andersen, K.K., Loft, S., Ketzel, M., Raaschou-Nielsen, O., 2010. Association between short-term exposure to ultrafine particles and hospital admissions for stroke in Copenhagen, Denmark. Eur. Heart J. 31, 2034–2040.

Atkinson, R., 2000. Atmospheric chemistry of VOCs and NOx. Atm. Environ. 34, 2063–2101.

Azimi, S., Rocher, V., Muler, M., Moilleron, R., Thevenot, D.R., 2005. Sources, distribution and variability of hydrocarbons and metals in atmospheric deposition in an urban area (Paris, France). Sci. Tot. Environ. 337, 223–239.

Bandowe, B.A., Meusel, H., Huang, R.-J., Ho, K., Cao, J., Hoffmann, T., Wilcke, W., 2014. $PM_{2.5}$-bound oxygenated PAHs, nitro-PAHs and parent-PAHs from the atmosphere of a Chinese megacity: Seasonal variation, sources and cancer risk assessment. Sci. Total Environ. 473–474, 77–87.

Bamford, H.A, Baker, J.E., 2003. Nitro-polycyclic aromatic hydrocarbon concentrations and sources in urban and sub-urban atmospheres of the Mid-Atlantic region. Atmos. Environ. 37, 2077–2091.

Barhoumi, B., Castro-Jiménez, J., Guigue, C., Goutx, M., Sempéré, R., Derouiche, A., Achour, A., Touil, S., Driss, M.R., Tedetti, M., 2018. Levels and risk assessment of hydrocarbons and organochlorines in aerosols from a North African coastal city (Bizerte, Tunisia). Environ. Pollut. 240, 422–431.

Barhoumi, B., Tedetti, M., Heimbürger-Boavida, L.-E., Tesan Onrubia, J.A., Dufour, A., Thi Doan, Q., Boutaleb, S., Touil, S., Scippo, M.-L., 2020b. Chemical composition and in vitro aryl hydrocarbon receptormediated activity of atmospheric particulate matter at an urban, agricultural and industrial site in North Africa (Bizerte, Tunisia). Chemosphere 258, 127312.

Barhoumi, B., Tedetti, M., Peris, A., Guigue, C., Aznar-Alemany, Ò., Touil, Driss, M.R., Eljarrat, E., 2020a. Halogenated flame retardants in atmospheric particles from a North African coastal city (Bizerte, Tunisia): Pollution characteristics and human exposure. Atmos. Pollut. Res. 11, 831–840.

Belleudi, V., Faustini, A., Stafoggia, M., Cattani, G., Marconi, A., Perucci, C.A., Forastiere, F., 2010. Impact of fine and ultrafine particles on emergency hospital admissions for cardiac and respiratory diseases. Epidemiology 21, 414–423.

Bi, X., Sheng, G., Peng, P., Chen, Y., Fu, J., 2005. Size distribution of n-alkanes and polycyclic aromatic hydrocarbons (PAHs) in urban and rural atmospheres of Guangzhou, China. Atmos. Environ. 39, 477–487.

Boström, C.-E., Gerde, P., Hanberg, A., Jernstrom, B., Johansson, C., Kyrklund, T., Rannug, A., Tornqvist, M., Victorin, K., Westerholm, R., 2002. Cancer risk assessment,

indicators, and guidelines for polycyclic aromatic hydrocarbons in the ambient air. Environ. Health Perspect. 110, 451–488.

CalEPA, 2020. California State Environmental Protection Agency. Office of Environmental Health Hazard Assessment. Available at *https://oehha.ca.gov/chemicals/*.

Caliskan, B., Kücük, A., Tasdemir, Y., Cindoruk, S.S., 2020. PAH levels in a furniture-manufacturing city atmosphere. Chemosphere 240, 124757.

Cao, R., Zhang, H., Geng, N., Fu, Q., Teng, M., Zou, L., Gao, Y., Chen, J., 2018. Diurnal variations of atmospheric polycyclic aromatic hydrocarbons (PAHs) during three sequent winter haze episodes in Beijing, China. Sci. Total Environ. 625, 1486–1493.

Castro Jiménez, J., Barhoumi, B., Paluselli, A., Tedetti, M., Jiménez, B., Muñoz-Arnanz, J., Wortham, H., Driss, M.R., Sempéré, R., 2017. Occurrence, loading and exposure of atmospheric particle-bound POPs at the African and European edges of the western Mediterranean Sea. Environ. Sci. Technol. 51, 13180–13189.

Chen, S., Liao, C., 2006. Health risk assessment on human exposed to environmental polycyclic aromatic hydrocarbons pollution sources. Sci. Total Environ. 366, 112–123.

Chirico, R., Spezzano, P., Cataldi, D., 2007. Gas–particle partitioning of polycyclic aromatic hydrocarbons during the spring and summer in a suburban site near major traffic arteries. Polycyc. Aromat. Comp. 27, 401–423.

Cincinelli, A., Del Bubba, M., Martellini, T., Gambaro, A., Lepri, L., 2007. Gas-particle concentration and distribution of n-alkanes and polycyclic aromatic hydrocarbons in the atmosphere of Prato (Italy). Chemosphere 68, 472–478.

Dachs, J., Eisenreich, S.J., 2000. Adsorption onto aerosol soot carbon dominates gaseparticle partitioning of polycyclic aromatic hydrocarbons. Environ. Sci. Technol. 34, 3690–3697.

Dachs, J., Méjanelle, L., 2010. Organic Pollutants in Coastal Waters, Sediments, and Biota: A Relevant Driver for Ecosystems During the Anthropocene? Estuaries Coast. 33, 1–14.

de Gouw, J.A., Middlebrook, A.M., Warneke, C., Ahmadov, R., Atlas, E.L., Bahreini, R., Blake, D.R., Brock, C.A., Brioude, J., Fahey, D.W., Fehsenfeld, F.C., Holloway, J.S., Le Henaff, M., Lueb, R.A., McKeen, S.A., Meagher, J.F., Murphy, D.M., Paris, C., Parrish, D.D., Perring, A.E., Pollack, I.B., Ravishankara, A.R., Robinson, A.L., Ryerson, T.B., Schwarz, J.P., Spackman, J.R., Srinivasan, A., Watts, L.A., 2011. Organic aerosol formation downwind from the deepwater horizon oil spill. Science 331, 1295–1299.

Ding, X., Wang, X.M., Xie, Z.Q., Xiang, C.H., Mai, B.X., Sun, L.G., Zheng, M., Sheng, G.Y., Fu, J.M., Poschl, U., 2007. Atmospheric polycyclic aromatic hydrocarbons observed over the North Pacific Ocean and the Arctic area: spatial distribution and source identification. Atmos. Environ. 41, 2061–2072.

Donahue, N.M., Kroll, J.H., Pandis, S.N., Robinson, A.L., 2012. A two-dimensional volatility basis set – Part 2: Diagnostics of organic-aerosol evolution. Atmos. Chem. Phys. 12, 615–634.

Duran, R., Cravo-Laureau, C., 2016. Role of environmental factors and microorganisms in determining the fate of polycyclic aromatic hydrocarbons in the marine environment. FEMS Microbiol. Rev. 40, 814–830.

Durant, J.L., Busby, Jr.W.F., Lafleur, A.L., Penman, B.W., Crespi, C.L., 1996. Human cell mutagenicity of oxygenated, nitrated and unsubstituted polycyclic aromatic hydrocarbons associated with urban aerosols. Mutat. Res. 371, 123–157.

Elorduy, I., Elcoroaristizabal, S., Durana, N., García, J.A., Alonso, L., 2016. Diurnal variation of particle-bound PAHs in an urban area of Spain using TD-GC/MS: influence of meteorological parameters and emission sources. Atmos. Environ. 138, 87–98.

Esen, F., Cindoruk, S.S., Tasdemir, Y., 2006. Ambient Concentrations and Gas/Particle Partitioning of Polycyclic Aromatic Hydrocarbons in an Urban Site in Turkey. Environ. Forensics 7, 303–312.

Fayiga, A.O., Ipinmoroti, M.O., Chirenje, T., 2018. Environmental pollution in Africa. Environ. Dev. Sustain. 20, 41–73.

Gaga, E.O., Ari, A., 2019. Gas-particle partitioning and health risk estimation of polycyclic aromatic hydrocarbons (PAHs) at urban, suburban and tunnel atmospheres: Use of measured EC and OC in model calculations. Atmos. Pollut. Res. 10, 1–11.

García-Martínez, M.J., Da Riva, I., Canoira, L., Llamas, J.F., Alcántara, R., Gallego, R.L.R., 2006. Photodegradation of polycyclic aromatic hydrocarbons in fossil fuels catalysed by supported TiO2. Appl. Catal. B-Environ. 67, 279–289.

Gong, P., Wang, X., Yao, T., 2011. Ambient distribution of particulate- and gas-phase n-alkanes and polycyclic aromatic hydrocarbons in the Tibetan Plate. Environ. Earth Sci. 64, 1703–1711.

González-Gaya, B., Martínez-Varela, A., Vila-Costa, M., Casal, P., Cerro-Gálvez, E., Berrojalbiz, N., Lundin, D., Vidal, M., Mompeán, C., Bode, A., Jiménez, B., Dachs J., 2019. Biodegradation as an important sink of aromatic hydrocabons in the ocean. Nat. Geosci. 12, 119–125.

Goss, K., Schwarzenbach, R.P., 1998. Gas/solid and gas/liquid partitioning of organic compounds: critical evaluation of the interpretation of equilibrium constant. Environ. Sci. Technol. 32, 2025–2032.

Guigue, C., Tedetti, M., Dang, D.H., Mullot, J.-U., Garnier, C., Goutx, M., 2017. Remobilization of polycyclic aromatic hydrocarbons and organic matter in seawater during sediment resuspension experiments from a polluted coastal environment: insights from Toulon Bay (France). Environ. Pollut. 229, 627–638.

Guigue, C., Tedetti, M., Ferretto, N., Garcia, N., Méjanelle, L., Goutx, M., 2014. Spatial and seasonal variabilities of dissolved hydrocarbons in surface waters from the Northwestern

Mediterranean Sea: Results from one year intensive sampling. Sci. Total. Environ. 466–467, 650–662.

Guigue, C., Tedetti, M., Giorgi, S., Goutx, M., 2011. Occurrence and distribution of hydrocarbons in the surface microlayer and subsurface water from the urban coastal marine area of Marseilles, Northwestern Mediterranean Sea. Mar. Pollut. Bull. 62, 2741–2752.

Harner, T., Bidleman, T.F., 1998. Octanol-air partition coefficient for describing particle/gas partitioning of aromatic compounds in urban air. Environ. Sci. Technol. 32, 1494–1502.

Hassan, S.K., Khoder, M.I., 2012. Gas-particle concentration, distribution, and health risk assessment of polycyclic aromatic hydrocarbons at a traffic area of Giza, Egypt. Environ. Monit. Assess. 184, 3593–612.

Honda, M., Suzuki, N., 2020. Toxicities of polycyclic aromatic hydrocarbons for aquatic animals. Int. J. Environ. Res. Public Health 17, 1363.

Hsu, H.-I., Lin, M.-Y., Chen, Y.-C., Chen, W.-Y., Yoon, C., Chen, M.-R., Tsai, P.-J., 2014. An integrated approach to assess exposure and health-risk from polycyclic aromatic hydrocarbons (PAHs) in a fastener manufacturing industry. Int. J. Environ. Res. Public Health 11, 9578–9594.

Iakovides, M., Apostolaki, M., Stephanou, E.G., 2021. PAHs, PCBs and organochlorine pesticides in the atmosphere of Eastern Mediterranean: Investigation of their occurrence, sources and gas-particle partitioning in relation to air mass transport pathways. Atmos. Environ. 244, 117931.

Ishtiaq, J., Syed, J.H., Jadoon, W.A., Hamid, N., Chaudhry, M.J.I., Shahnawaz, M., Nasir, J., Rizvi, S.H.H., Chakraborty, P., Li, J., Zhang, G., 2021. Atmospheric polycyclic aromatic hydrocarbons (PAHs) at urban settings in Pakistan: Spatial variations, sources and health risks. Chemosphere 274, 129811.

Jolley, R.L., Wang, R.G.M., 1992. Effective and safe waste management: Interfacing Sciences and Engineering with Monitoring and Risk Analysis. Lewis Publishers.

Kim, J.Y., Lee, J.Y., Choi, S.-D., Kim, Y.P., Ghim, Y.S., 2012. Gaseous and particulate polycyclic aromatic hydrocarbons at the Gosan background site in East Asia. Atmos. Environ. 49, 311–319.

Lei, Y.D., Chankalal, R., Chan, A., Wania, F., 2002. Supercooled Liquid Vapor Pressures of the Polycyclic Aromatic Hydrocarbons, J. Chem. Eng. Data 47, 801–806.

Li, J., Li, K., Li, H., Wang, X., Wang, W., Wang, K., Ge, M., 2022. Long-chain alkanes in the atmosphere: A review. J. Environ. Sci. 114, 37–52.

Liggio, J., Li, S.-M., Hayden, K., Taha, Y.M., Craig Stroud, C., Darlington, A., Drollette, B.D., Gordon, M., Lee, P., Liu, P., Leithead, A., Moussa, S.G., Wang, D., O'Brien, J., Mittermeier, R.L., Brook, J.R., Lu, G., Staebler, R.M., Han, Y., Tokarek, T.W., Osthoff, H.D., Makar, P.A., Zhang, J., Plata, D.L., Gentner, D.R., 2016. Oil sands operations as a large source of secondary organic aerosols. Nature 534 (7605), 91.

Lin, H., Tao, J., Du, Y., Liu, T., Qian, Z., Tian, L., Di, Q., Rutherford, S., Guo, L., Zeng, W., Xiao, J., Li, X., He, Z., Xu, Y., Ma, W., 2016. Particle size and chemical constituents of ambient particulate pollution associated with cardiovascular mortality in Guangzhou, China. Environ. Pollut. 208, 758–766.

Liu, L., Breitner, S., Schneider, A., Cyrys, J., Brüske, I., Franck, U., Schlink, U., Marian Leitte, A., Herbarth, O., Wiedensohler, A., 2013. Size-fractioned particulate air pollution and cardiovascular emergency room visits in Beijing, China. Environ. Res. 121, 52–63.

Liu, H., Man, H., Cui, H., Wang, Y., Deng, F., Wang, Y., Yang, X., Xiao, Q., Zhang, Q., Yan Ding, Y., He, K., 2017. An updated emission inventory of vehicular VOCs and IVOCs in China. Atmos. Chem. Phys. 17, 12709–12724 .

Luo, H., Jia, L., Wan, Q., An, T., Wang, Y., 2019. Role of liquid water in the formation of O_3 and SOA particles from 1,2,3-trimethylbenzene. Atmos. Environ. 217, 116955.

Ma, W.-L., Sun, D.-Z., Shen, W.-G., Yang, M., Qi, H., Liu, L.-Y., Shen, J.-M., Li, Y.-F., 2011. Atmospheric concentrations, sources and gas-particle partitioning of PAHs in Beijing after the 29th Olympic Games. Environ. Pollut. 159, 1794–1801.

Ma, W.-L., Zhu, F.-J., Liu, L.-Y., Jia, H.-L., Yang, M., Li, Y.-F., 2019. PAHs in Chinese atmosphere: Gas/particle partitioning. Sci. Total Environ. 693, 133623.

Mandalakis, M., Tsapakis, M., Tsoga, A., Stephanou, E.G., 2002. Gas–particle concentrations and distribution of aliphatic hydrocarbons, PAHs, PCBs and PCDD/Fs in the atmosphere of Athens (Greece). Atmos. Environ. 36, 4023–4035.

Manisalidis, I., Stavropoulou, E., Stavropoulos, A., Bezirtzoglou, E., 2020. Environmental and Health Impacts of Air Pollution: A review. Front. Public Health *https://doi.org/10.3389/fpubh.2020.00014*.

Manoli, E., Kouras, A., Karagkiozidou, O., Argyropoulos, G., Voutsa, D., Samara, C., 2016. Polycyclic aromatic hydrocarbons (PAHs) at traffic and urban background sites of northern Greece: Source apportionment of ambient PAH levels and PAH-induced lung cancer risk. Environ. Sci. Pollut. Res. 23, 3556–3568.

Meng, X., Ma, Y., Chen, R., Zhou, Z., Chen, B., Kan, H., 2013. Size-fractionated particle number concentrations and daily mortality in a Chinese city. Environ. Health Perspect. 121, 1174–1178.

Mulder, M.D., Dumanoglu, Y., Efstathiou, C., Kukučka, P., Matejovičová, J., Maurer, C., Přibylová, P., Prokeš, R., Sofuoglu, A., Sofuoglu, S., Wilson, J., Zetzsch, C., Wotawa, G., Lammel, G., 2019. Fast formation of nitro-PAHs in the marine atmosphere constrained in a regional-scale Lagrangian field experiment. Environ. Sci. Technol. 53, 15, 8914–8924.

Munyeza, C.F., Rohwer, E.R., Forbes, P.B.C., 2019. A review of monitoring of airborne polycyclic aromatic hydrocarbons: An African perspective. Trends Environ. Anal. Chem. 24, e00070.

Nisbet, I.C.T., LaGoy, P.K., 1992. Toxic equivalency factors (TEFs) for polycyclic aromatic hydrocarbons (PAHs). Regul. Toxicol. Pharmacol. 16, 290–300.

Pandis, S.N., Donahue, N.M., Murphy, B.N., Riipinen, I., Fountoukis, C., Karnezi, E., Patoulias, D., Skyllakou, K., 2013. Introductory lecture: Atmospheric organic aerosols: insights from the combination of measurements and chemical transport models. Faraday Discuss. 165, 9–24.

Pankow, J.F., 1994a. An absorption model of gas/particle partitioning of organic compounds in the atmosphere. Atmos. Environ. 28, 185–188.

Pankow, J.F., 1994b. An absorption model of the gas/aerosol partitioning involved in the formation of secondary organic aerosol. Atmos. Environ. 28, 189–193.

Parnis, J.M., Mackay, D., Harner, T., 2015. Temperature dependence of Henry's law constants and KOA for simple and heteroatom-substituted PAHs by COSMO-RS. Atmos. Environ. 110, 27–35.

Peng, C., Chen, W., Liao, X., Wang, M., Ouyang, Z., Jiao, W., Bai, Y., 2011. Polycyclic aromatic hydrocarbons in urban soils of Beijing: status, sources, distribution and potential risk. Environ. Pollut. 159, 802–808.

Ramírez, N., Cuadras, A., Rovira, E., Marcé, R.M., Borrull, F., 2011. Risk assessment related to atmospheric polycyclic aromatic hydrocarbons in gas and particle phases near industrial sites. Environ. Health Perspect. 119, 1110–1116.

Ravindra, K., Sokhi, R., Van Grieken, R., 2008. Atmospheric polycyclic aromatic hydrocarbons: source attribution, emission factors and regulation. Atmos. Environ. 42, 2895–2921.

Reisen, F., Arey, J., 2005. Atmospheric reactions influence seasonal PAH and nitro-PAH concentrations in the Los Angeles basin. Environ. Sci. Technol. 39, 64–73.

Robinson, A.L., Donahue, N.M., Shrivastava, M.K., Weitkamp, E.A., Sage, A.M., Andrew P. Grieshop, A.P., Lane, T.E., Pierce, J.R., Pandis, S.N., 2007. Rethinking Organic Aerosols: Semivolatile Emissions and Photochemical Aging. Science 315, 1259–1262.

Schauer, J.J., Kleeman, M.J., Cass, G.R., Simoneit, B.R.T., 1999. Measurement of emissions from air pollution sources. 2. C1 through C30 organic compounds from medium duty diesel trucks. Environ. Sci. Technol. 33, 1578–1587.

Schauer, J.J., Kleeman, M.J., Cass, G.R., Simoneit, B.R.T., 2001. Measurement of emissions from air pollution sources. 3. C1-C29 organic compounds from fireplace combustion of wood. Environ. Sci. Technol. 35, 1716–1728.

Schauer, J.J., Kleeman, M.J., Cass, G.R., Simoneit, B.R.T., 2002. Measurement of emissions from air pollution sources. 5. C1-C32 organic compounds from gasoline-powered motor vehicles. Environ. Sci. Technol. 36, 1169–1180.

Sharma, H., Jain, V.K., Khan, Z.H., 2007. Characterization and source identification of polycyclic aromatic hydrocarbons (PAHs) in the urban environment of Delhi. Chemosphere 66, 302–310.

Shen, G., Tao, S., Wei, S., Chen, Y., Zhang, Y., Shen, H., Huang, Y., Zhu, D., Yuan, C., Wang, H., Wang, Y., Pei, L., Liao, Y., Duan, Y., Wang, B., Wang, R., Lv, Y., Li, W., Wang, X., Zheng, X., 2013. Field measurement of emission factors of PM, EC, OC, parent, nitro-, and oxy-polycyclic aromatic hydrocarbons for residential briquette, coal cake, and wood in rural Shanxi, China. Environ. Sci. Technol. 47, 2998–3005.

Shi, B., Wang, W., Zhou, L., Li, J., Wang, J., Chen, Y., Zhang, W., Ge, M., 2019a. Kinetics and mechanisms of the gas-phase reactions of OH radicals with three C_{15} alkanes. Atmos. Environ. 207, 75–81.

Shi, B., Wang, W., Zhou, L., Sun, Z., Fan, C., Chen, Y., Zhang, W., Qiao, Y., Qiao, Y., Ge, M., 2019b. Atmospheric oxidation of C10~14 n-alkanes initiated by Cl atoms: Kinetics and mechanism. Atmos. Environ. 222, 117–166.

Simcik, M.F., Franz, T.P., Zhang, H., Eisenreich, S.J., 1998. Gas–particle partitioning of PCBs and PAHs in the Chicago urban and adjacent coastal atmosphere: states of equilibrium. Environ. Sci. Technol. 32, 251–257.

Simoneit, B.R.T., 2002. Biomass burning — a review of organic tracers for smoke from incomplete combustion. Appl. Geochem. 17, 129–162.

Su, Y., Lei, Y.D., Wania, F., Shoeib, M., Harner, T., 2006. Regressing Gas/Particle Partitioning Data for Polycyclic Aromatic Hydrocarbons. Environ. Sci. Technol. 40, 11, 3558–3564.

Terzi, E., Samara, C., 2004. Gas-Particle Partitioning of Polycyclic Aromatic Hydrocarbons in Urban, Adjacent Coastal, and Continental Background Sites of Western Greece. Environ. Sci. Technol. 38, 4973–4978.

Tomaz, S., Shahpoury, P., Jaffrezo, J.-L., Lammel, G., Perraudin, E., Villenave, E., Albinet, A., 2016. One-year study of polycyclic aromatic compounds at an urban site in Grenoble (France): Seasonal variations, gas/particle partitioning and cancer risk estimation. Sci. Total Environ. 565, 1071–1083.

Tsapakis, M., Stephanou, E.G., 2005. Occurrence of gaseous and particulate polycyclic aromatic hydrocarbons in the urban atmosphere: study of sources and ambient temperature effect on the gas/particle concentration and distribution. Environ. Pollut. 133, 147–156.

US EPA, 2005. EPA-CMB8.2 Model Code. Available at *https://www.epa.gov/scram/chemical-mass-balance-cmb-model*.

Valavanidis, A., Iliopoulos, N., Gotsis, G., Fiotakis, K., 2008. Persistent free radicals, heavy metals and PAHs generated in particulate soot emissions and residue ash from controlled combustion of common types of plastic. J. Hazard. Mater. 156, 277–284.

Vardar, N., Tasdemir, Y., Odabasi, M., Noll, K.E., 2004. Characterization of atmospheric concentrations and partitioning of PAHs in the Chicago atmosphere. Sci. Total Environ. 327, 163–174.

Vasilakos, C., Levi, N., Maggos, T., Hatzianestis, J., Michopoulos, J., Helmis, C., 2007. Gas–particle concentration and characterization of sources of PAHs in the atmosphere of a suburban area in Athens, Greece. J. Hazard. Mater. 140, 45–51.

Volckens, J., Leith, D., 2003. Comparison of methods for measuring gas–particle partitioning of semi-volatile compounds. Atmos. Environ. 37, 3177–3188.

Vuong, Q.T., Son, J.-M., Thang, P.Q., Ohura, T., Choi. S.-D., 2022. Application of gas chromatographic retention times to determine physicochemical properties of nitrated, oxygenated, and parent polycyclic aromatic hydrocarbons. Environ. Pollut. 294, 118644.

Wang, W., Simonich, S.L.M., Wang, W., Giri, B., Zhao, J., Xue, M., Cao, J., Lu, X., Tao, S., 2011. Atmospheric polycyclic aromatic hydrocarbon concentrations and gas/particle partitioning at background, rural village and urban sites in the North China Plain. Atmos. Res. 99, 197–206.

Wang, Z., Fingas, M., Page, D.S., 1999. Oil spill identification. J. Chromatogr. A 843, 369–411.

Wang, Z., Na, G., Ma, X., Fang, X., Ge, L., Gao, H., Yao, Z., 2013. Occurrence and gas/particle partitioning of PAHs in the atmosphere from the North Pacific to the Arctic Ocean. Atmos. Environ. 2013, 77, 640–646.

Weinstein, J.E., Crawford, K.D., Garner, T.R., Flemming, A.J., 2010. Screening-level ecological and human health risk assessment of polycyclic aromatic hydrocarbons in

stormwater detention pond sediments of Coastal South Carolina, USA. J. Hazard. Mater. 178, 906–916.

WHO, 1987. World Health Organization. Air quality guidelines for Europe. Copenhagen, Denmark.

Xie, M., Hannigan, M.P., Barsanti, K.C., 2014. Gas/particle partitioning of n-alkanes, PAHs and oxygenated PAHs in urban Denver. Atmos. Environ. 95, 355–362.

Yadav, S., Tandon, A., Attri, A.K., 2013. Monthly and seasonal variations in aerosol associated n-alkane profiles in relation to meteorological parameters in New Delhi, India. Aerosol Air Qual. Res. 13, 287–300.

Yuan, B., Hu, W.W., Shao, M., Wang, M., Chen, W.T., Lu, S.H., Zeng, L.M., Hu, M., 2013. VOC emissions, evolutions and contributions to SOA formation at a receptor site in eastern China. Atmos. Chem. Phys. 13, 8815–8832.

Zhao, Y., Hennigan, C.J., May, A.A., Tkacik, D.S., de Gouw, J.A., Gilman, J.B., Kuster, W.C., Borbon, A., Robinson, A.L., 2014. Intermediate-volatility organic compounds: a large source of secondary organic aerosol. Environ. Sci. Technol. 48, 13743–13750.

Zhao, Y., Nguyen, N.T., Presto, A.A., Hennigan, C.J., May, A.A., Robinson, A.L., 2015. Intermediate volatility organic compound emissions from on-road diesel vehicles: Chemical composition, emission factors, and estimated secondary organic aerosol production. Environ. Sci. Technol. 49, 11516–11526.

Figure captions

Figure 1. a) Concentrations of total (Σ_{34}) PAHs (ng m^{-3}) from March 2015 to January 2016, b) annual mean concentrations of individual PAHs (ng m^{-3}), and c) relative abundances of individual PAHs (%) in the atmospheric gas and particle phases of Bizerte city. The particle-phase data used is from Barhoumi et al. (2018).

Figure 2. a) Concentrations of total (Σ_{28}) AHs (ng m^{-3}) from March 2015 to January 2016, b) annual mean concentrations of individual AHs (ng m^{-3}), and c) relative abundances (%) of individual AHs in the atmospheric gas and particle phases of Bizerte city. The particle-phase data used is from Barhoumi et al. (2018).

Figure 3. Regression plots of a) log K_p *versus* log P_L^0 for PAHs, b) log K_p *versus* log K_{OA} for PAHs, and c) log K_p *versus* log P_L^0 for AHs in atmospheric samples from Bizerte city. Blue dots represent the compounds used for the regression, i.e. DBT, Phe, Ant, Flu, Pyr, BaA, Chr, BbF, BkF, BeP, BaP and BghiP for PAHs and *n*-C_{19}-*n*-C_{35} for AHs. Red dots represent the compounds excluded from the regressions, i.e. Nap, Acy and Fl for PAHs and *n*-C_{15}-*n*-C_{18}, Pr and Phy for AHs.

Figure 4. a) Concentrations of benzo[*a*]pyrene toxic equivalency quotient (BaP-TEQ, in ng m^{-3}), and b) relative contribution of gas and particle-bound PAHs to the BaP-TEQ concentrations in the atmospheric gas and particle phases of Bizerte city from March 2015 to January 2016. The black dotted line represents the WHO reference threshold (1 ng m^{-3}).

Figure 5. Cumulative distribution function of incremental lifetime cancer risk (ILCR) associated with exposure to PAHs present in both gas and particle phases of outdoor air in Bizerte city evaluated for the period of March 2015 to January 2016.

Table captions

Table 1. Mean PAH concentrations (ng m^{-3}) in the gas phase of Bizerte city during the warm season (March–August 2015), the cold season (September 2015–January 2016), and over the whole year (March 2015–January 2016).

Table 2. Mean AH concentrations (ng m^{-3}) in the gas phase of Bizerte city during the warm season (March–August 2015), the cold season (September 2015–January 2016), and over the whole year (March 2015–January 2016).

Table 3. Assessment of incremental lifetime cancer risk (ILCR) stratified by specific age-groups and season for PAHs (calculated for the gas + particle phases).

Table 1

Mean PAH concentrations (ng m^{-3}) in the gas phase of Bizerte city during the warm season (March–August 2015), the cold season (September 2015–January 2016), and over the whole year (March 2015–January 2016).

Compound	Gas phase (ng m^{-3})		
	Warm	Cold	Annual
Nap [a]	0.034 ± 0.063	0.078 ± 0.133	0.048 ± 0.093
Acy [a]	0.042 ± 0.056	0.266 ± 0.865	0.114 ± 0.493
Ace [a]	0.004 ± 0.009	0.024 ± 0.052	0.010 ± 0.031
Fl [a]	0.128 ± 0.123	0.605 ± 0.841	0.281 ± 0.527
DBT [b]	0.233 ± 0.280	0.259 ± 0.207	0.241 ± 0.257
Phe [a]	2.414 ± 2.234	8.579 ± 9.924	4.391 ± 3.407
Ant [a]	0.141 ± 0.118	0.547 ± 0.571	0.271 ± 0.382
Flu [a]	0.832 ± 0.420	1.933 ± 1.210	1.185 ± 0.916
Pyr [a]	0.890 ± 0.397	2.030 ± 1.021	1.255 ± 0.846
BaA [a]	0.018 ± 0.020	0.081 ± 0.131	0.038 ± 0.080
Chr [a]	0.082 ± 0.071	0.287 ± 0.378	0.148 ± 0.238
BbF [a]	0.006 ± 0.006	0.015 ± 0.010	0.009 ± 0.008
BkF [a]	0.002 ± 0.003	0.006 ± 0.005	0.003 ± 0.004
BeP [b]	0.004 ± 0.004	0.011 ± 0.006	0.007 ± 0.006
BaP [a]	0.002 ± 0.004	0.005 ± 0.005	0.003 ± 0.004
Per [b]	nd	nd	nd
DahA [a]	nd	nd	nd
IcdP [a]	0.001 ± 0.002	0.002 ±	0.001 ± 0.002
BghiP [a]	0.002 ± 0.003	0.004 ±	0.002 ± 0.003
C1-Nap [c]	0.054 ± 0.071	0.121 ± 0.183	0.076 ± 0.121
C2-Nap [c]	0.207 ± 0.286	0.565 ± 0.804	0.322 ± 0.531
C3-Nap [c]	0.391 ± 0.412	1.070 ± 1.277	0.609 ± 0.848
C1-Fl [c]	0.320 ± 0.232	1.415 ± 1.816	0.671 ± 1.148
C2-Fl [c]	0.663 ± 0.430	1.623 ± 1.357	0.971 ± 0.946
C3-Fl [c]	0.937 ± 0.425	2.000 ± 1.242	1.278 ± 0.921
C1-Phe/Ant [c]	2.814 ± 1.382	6.764 ± 4.721	4.081 ± 3.407
C2-Phe/Ant [c]	1.948 ± 0.908	3.111 ± 1.193	2.321 ± 1.137
C3-Phe/Ant [c]	0.997 ± 0.413	1.575 ± 0.633	1.169 ± 0.564
C1-Flu/Pyr [c]	0.349 ± 0.200	0.681 ± 0.316	0.456 ± 0.286
C2-Flu/-Pyr [c]	0.217 ± 0.155	0.538 ± 0.452	0.320 ± 0.320
C3-Flu/-Pyr [c]	0.026 ± 0.034	0.111 ± 0.164	0.054 ± 0.103
C1-BaA/Chr [c]	0.036 ± 0.034	0.082 ± 0.132	0.051 ± 0.082
C2-BaA/Chr [c]	0.002 ± 0.005	0.014 ± 0.047	0.006 ± 0.027
C3-BaA/Chr [c]	nd	nd	nd
Σ_{16}EPA-PAHs	4.6 ± 2.8	14.5 ± 12.8	7.8 ± 8.8
Σ_{34}PAHs (parent + alkylated)	13.8 ± 6.6	34.4 ± 23.7	20.4 ± 17.2
Alk/Par	2.3 ± 0.7	1.8 ± 0.7	2.1 ± 0.7

nd: not detected; [a,b] parent PAHs; [a] EPA priority PAHs; [c] Alkylated PAHs.

Table 2

Mean AH concentrations (ng m^{-3}) in the gas phase of Bizerte city during the warm season (March–August 2015), the cold season (September 2015–January 2016) and over the whole year (March 2015–January 2016).

Compound	Abbreviation	Gas phase (ng m^{-3})		
		Warm	Cold	Annual
Pentadecane	C_{15}	0.014 ± 0.054	0.038 ± 0.083	0.022 ± 0.065
Hexadecane	C_{16}	0.052 ± 0.134	0.145 ± 0.250	0.082 ± 0.182
Heptadecane	C_{17}	0.695 ± 1.907	0.576 ± 0.635	0.656 ± 1.605
Octadecane	C_{18}	1.012 ± 0.470	1.291 ± 0.877	1.101 ± 0.635
Nonadecane	C_{19}	1.440 ± 0.672	2.125 ± 1.318	1.659 ± 0.971
Eicosane	C_{20}	3.565 ± 0.739	3.800 ± 1.132	3.640 ± 0.880
Heneicosane	C_{21}	2.830 ± 0.611	3.573 ± 0.905	3.069 ± 0.791
Docosane	C_{22}	4.048 ± 1.764	3.737 ± 1.132	3.949 ± 1.584
Tricosane	C_{23}	2.387 ± 0.853	2.516 ± 0.893	2.429 ± 0.859
Tetracosane	C_{24}	1.923 ± 1.015	1.761 ± 0.994	1.871 ± 1.002
Pentacosane	C_{25}	1.149 ± 0.706	0.984 ± 0.752	1.096 ± 0.718
Hexacosane	C_{26}	0.551 ± 0.485	0.535 ± 0.462	0.546 ± 0.473
Heptacosane	C_{27}	0.552 ± 0.515	0.491 ± 0.412	0.533 ± 0.481
Octacosane	C_{28}	0.254 ± 0.449	0.212 ± 0.244	0.241 ± 0.393
Nonacosane	C_{29}	0.303 ± 0.417	0.251 ± 0.252	0.286 ± 0.370
Triacontane	C_{30}	0.131 ± 0.319	0.116 ± 0.169	0.126 ± 0.278
Hentriacontane	C_{31}	0.196 ± 0.284	0.166 ± 0.158	0.186 ± 0.249
Dotriacontane	C_{32}	0.053 ± 0.124	0.060 ± 0.075	0.056 ± 0.110
Tritriacontane	C_{33}	0.044 ± 0.057	0.067 ± 0.063	0.051 ± 0.059
Tetratriacontane	C_{34}	0.015 ± 0.024	0.026 ± 0.036	0.018 ± 0.029
Pentatriacontane	C_{35}	0.008 ± 0.015	0.021 ± 0.030	0.012 ± 0.022
Hexatriacontane	C_{36}	0.004 ± 0.009	0.014 ± 0.025	0.007 ± 0.017
Heptatriacontane	C_{37}	0.002 ± 0.006	0.010 ± 0.027	0.005 ± 0.016
Octatriacontane	C_{38}	0.002 ± 0.006	0.008 ± 0.021	0.004 ± 0.013
Nonatriacontane	C_{39}	0.001 ± 0.005	0.007 ± 0.023	0.003 ± 0.014
Tetracontane	C_{40}	nd	0.006 ± 0.018	0.002 ± 0.010
Pristane	Pr	0.230 ± 0.219	0.497 ± 0.760	0.315 ± 0.475
Phytane	Phy	0.507 ± 0.352	0.638 ± 0.478	0.549 ± 0.397
Σ_{28}AHs		22.0 ± 4.9	23.7 ± 6.1	22.5 ± 5.3
UCM		90.4 ± 33.2	91.3 ± 26.2	90.7 ± 30.9
UCM/R		4.2 ± 1.7	3.9 ± 0.8	4.1 ± 1.5

nd: not detected.

Table 3 Assessment of incremental lifetime cancer risk (ILCR) stratified by specific age-groups and season for PAHs (calculated for the gas + particle phases).

Age group	Season	Estimated ILCR	Predicted ILCR by Monte Carlo simulation					
		Mean	Mean ± SD	5th	25th	50th	75th	95th
Infants	Warm	1.6×10^{-6}	$1.7\times10^{-6} \pm 1.3\times10^{-6}$	4.0×10^{-7}	8.2×10^{-7}	1.3×10^{-6}	2.1×10^{-6}	4.1×10^{-6}
Children	Warm	1.7×10^{-5}	$1.7\times10^{-5} \pm 1.2\times10^{-5}$	4.9×10^{-6}	9.0×10^{-6}	1.4×10^{-5}	2.2×10^{-5}	4.0×10^{-5}
Adolescents	Warm	1.1×10^{-5}	$1.1\times10^{-5} \pm 7.5\times10^{-6}$	3.2×10^{-6}	5.9×10^{-6}	9.0×10^{-6}	1.4×10^{-5}	2.5×10^{-5}
Adults	Warm	5.2×10^{-5}	$5.2\times10^{-5} \pm 3.7\times10^{-5}$	1.5×10^{-5}	2.8×10^{-5}	4.3×10^{-5}	6.6×10^{-5}	1.2×10^{-4}
Infants	Cold	4.5×10^{-6}	$4.7\times10^{-6} \pm 5.1\times10^{-6}$	6.6×10^{-7}	1.7×10^{-6}	3.1×10^{-6}	5.8×10^{-6}	1.4×10^{-5}
Children	Cold	4.7×10^{-5}	$4.8\times10^{-5} \pm 5.2\times10^{-5}$	7.6×10^{-6}	1.8×10^{-5}	3.3×10^{-5}	5.9×10^{-5}	1.4×10^{-4}
Adolescents	Cold	3.0×10^{-5}	$3.1\times10^{-5} \pm 3.3\times10^{-5}$	6.1×10^{-6}	1.2×10^{-5}	2.1×10^{-5}	3.7×10^{-5}	8.9×10^{-5}
Adults	Cold	1.5×10^{-4}	$1.4\times10^{-4} \pm 1.5\times10^{-4}$	2.4×10^{-5}	5.6×10^{-5}	9.9×10^{-5}	1.8×10^{-4}	4.1×10^{-4}
Infants	Annual	2.5×10^{-6}	$2.6\times10^{-6} \pm 3.3\times10^{-6}$	3.0×10^{-7}	7.9×10^{-7}	1.6×10^{-6}	3.2×10^{-6}	8.2×10^{-6}
Children	Annual	2.7×10^{-5}	$2.7\times10^{-5} \pm 3.3\times10^{-5}$	3.4×10^{-6}	8.8×10^{-6}	1.7×10^{-5}	3.3×10^{-5}	8.2×10^{-5}
Adolescents	Annual	1.7×10^{-5}	$1.7\times10^{-5} \pm 2.2\times10^{-5}$	2.2×10^{-6}	5.7×10^{-6}	1.1×10^{-5}	2.1×10^{-5}	5.2×10^{-5}
Adults	Annual	8.2×10^{-5}	$8.3\times10^{-5} \pm 1.1\times10^{-4}$	1.1×10^{-5}	2.8×10^{-5}	5.3×10^{-5}	1.0×10^{-4}	2.6×10^{-4}

SD = Standard deviation. 5th, 25th, 50th, 75th, and 95th Percentiles.

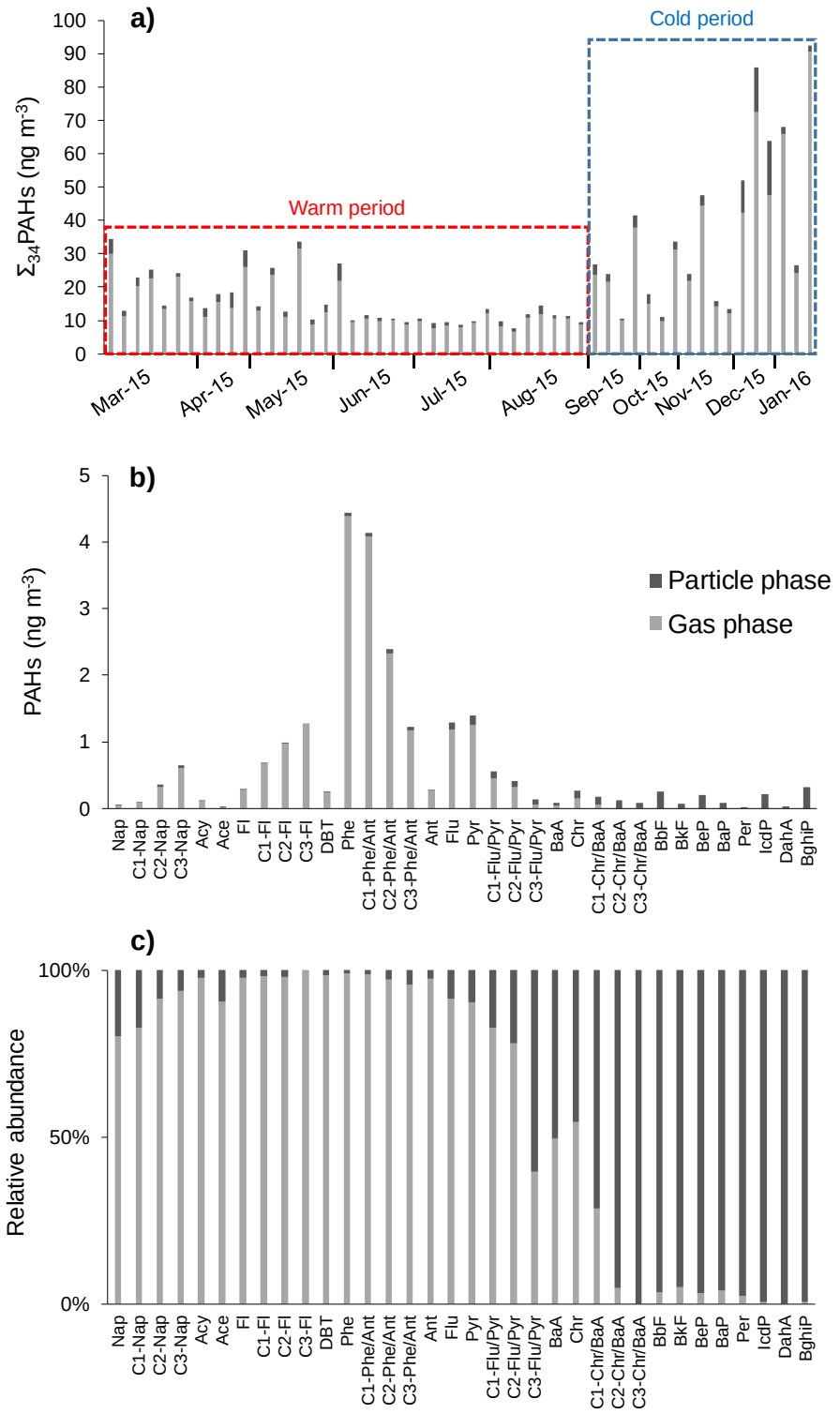

Fig. 1. a) Concentrations of total (Σ_{34}) PAHs (ng m^{-3}) from March 2015 to January 2016, b) annual mean concentrations of individual PAHs (ng m^{-3}), and c) relative abundances of individual PAHs (%) in the atmospheric gas and particle phases of Bizerte city. The particle-phase data used is from Barhoumi et al. (2018).

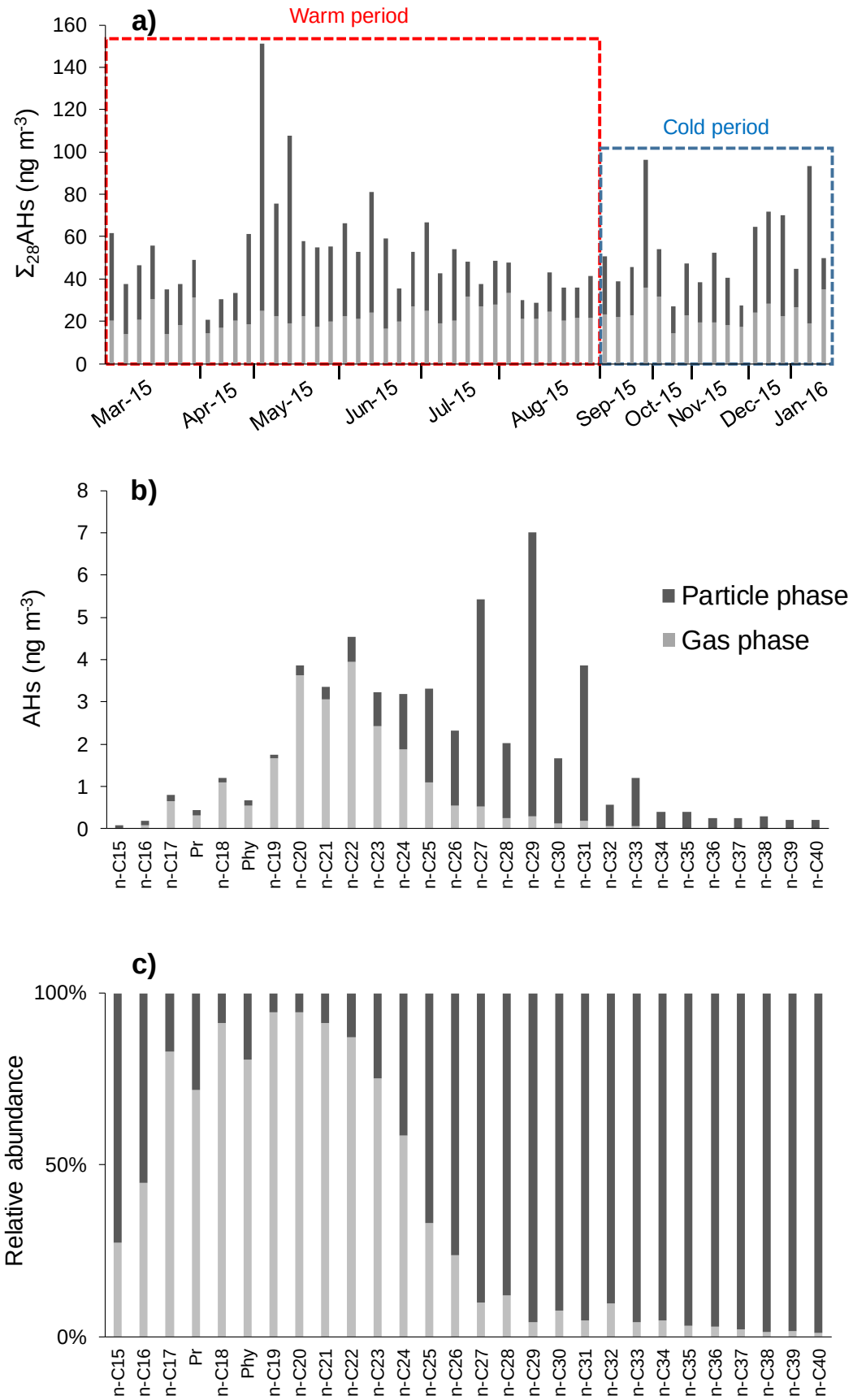

Fig. 2. a) Concentrations of total (Σ_{28}) AHs (ng m^{-3}) from March 2015 to January 2016, b) annual mean concentrations of individual AHs (ng m^{-3}), and c) relative abundances (%) of individual AHs in the atmospheric gas and particle phases of Bizerte city. The particle-phase data used is from Barhoumi et al. (2018).

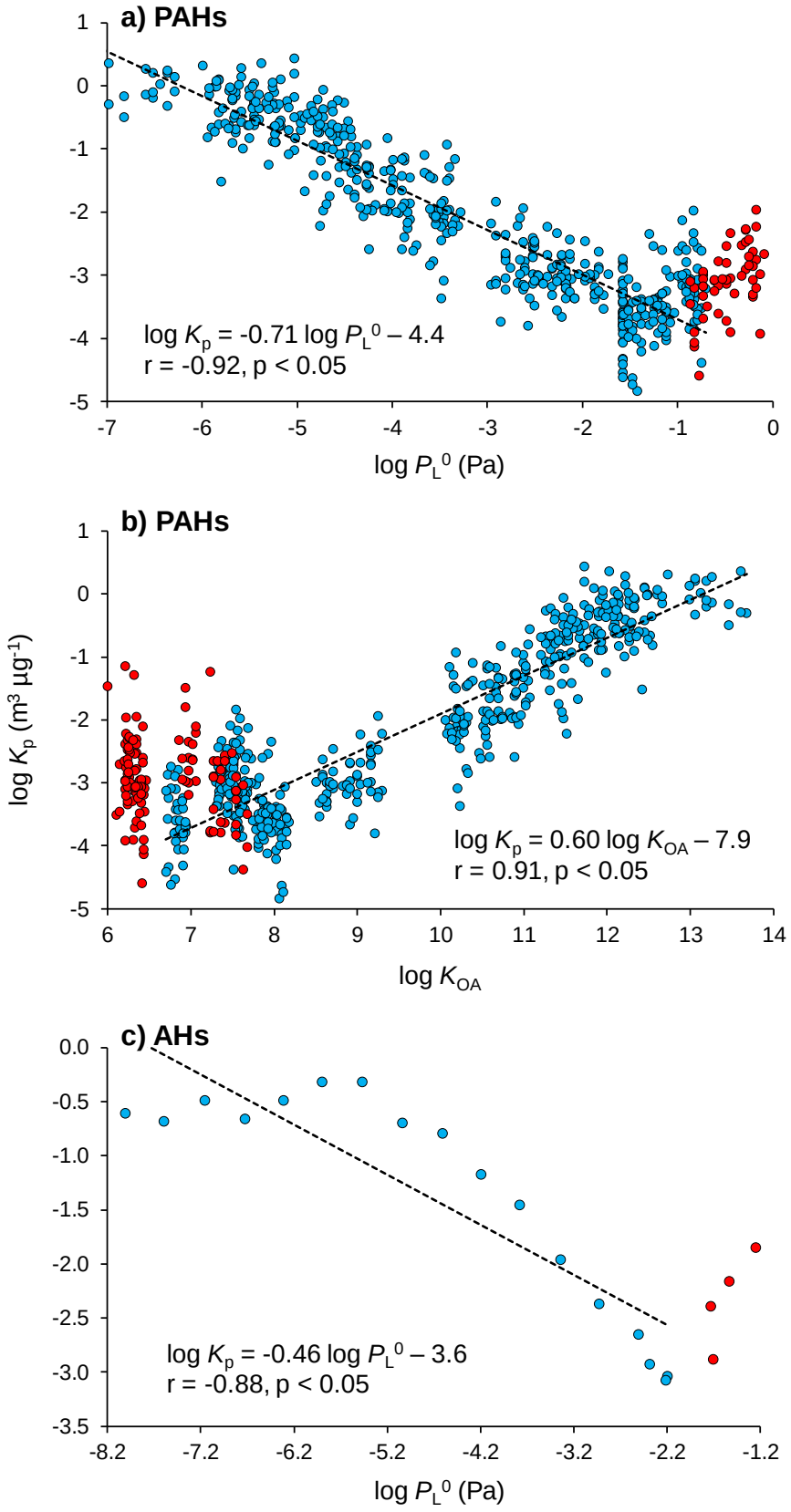

Fig. 3. Regression plots of a) log K_p *versus* log P_L^0 for PAHs, b) log K_p *versus* log K_{OA} for PAHs, and c) log K_p *versus* log P_L^0 for AHs in atmospheric samples from Bizerte city. Blue dots represent the compounds used for the regression, i.e. DBT, Phe, Ant, Flu, Pyr, BaA, Chr, BbF, BkF, BeP, BaP and BghiP for PAHs and *n*-C_{19}-*n*-C_{35} for AHs. Red dots represent the compounds excluded from the regressions, i.e. Nap, Acy and Fl for PAHs and *n*-C_{15}-*n*-C_{18}, Pr and Phy for AHs.

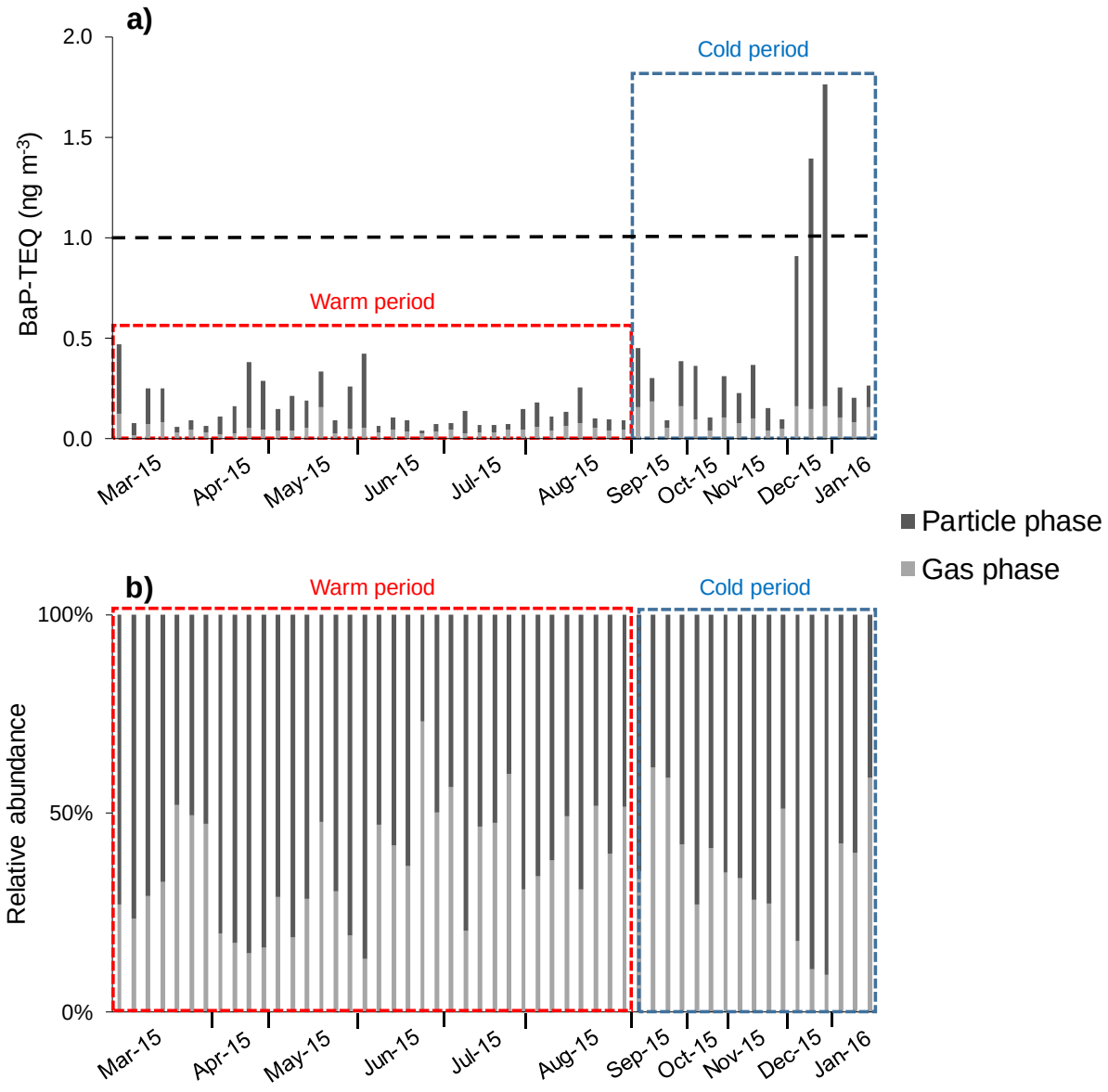

Fig. 4. a) Concentrations of benzo[a]pyrene toxic equivalency quotient (BaP-TEQ, in ng m^{-3}), and b) relative contribution of gas and particle-bound PAHs to the BaP-TEQ concentrations in the atmospheric gas and particle phases of Bizerte city from March 2015 to January 2016. The black dotted line represents the WHO reference threshold (1 ng m^{-3}).

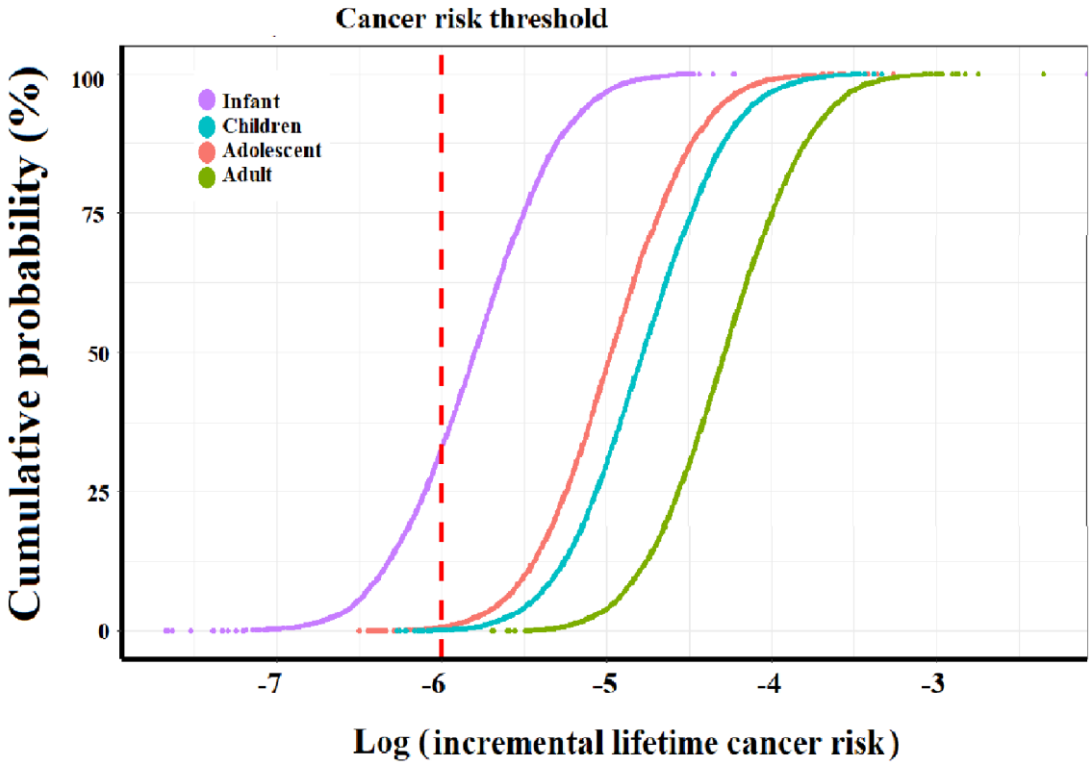

Fig. 5. Cumulative distribution function of incremental lifetime cancer risk (ILCR) associated with exposure to PAHs present in both gas and particle phases of outdoor air in Bizerte city evaluated for the period of March 2015 to January 2016.

SUPPLEMENTARY INFORMATION

Hydrocarbons in the atmospheric gas phase of a coastal city in Tunisia: levels, gas–particle partitioning, and health risk assessment

Badreddine Barhoumi[a, b, *], Catherine Guigue[b], Soufiane Touil[a], Boris Johnson-Restrepo[c], Mohamed Ridha Driss[a], Marc Tedetti[b, *]

[a] *Laboratory of Hetero-Organic Compounds and Nanostructured Materials (LR18ES11), Department of Chemistry, Faculty of Sciences of Bizerte, University of Carthage, 7021 Zarzouna, Tunisia*

[b] *Aix Marseille Univ., Université de Toulon, CNRS, IRD, MIO UM 110, 13288, Marseille, France*

[c]*Environmental Chemistry Research Group, School of Exact and Natural Sciences, University Campus of San Pablo, University of Cartagena, Zaragocilla, Carrera 50 No. 24–99, Cartagena, 130015, Colombia*

*Corresponding authors

E-mail: barhoumibadredine@yahoo.fr

E-mail: marc.tedetti@mio.osupytheas.fr

The supplementary information contains 15 pages and includes 7 tables and 3 figures.

List of contents of the supplementary information:

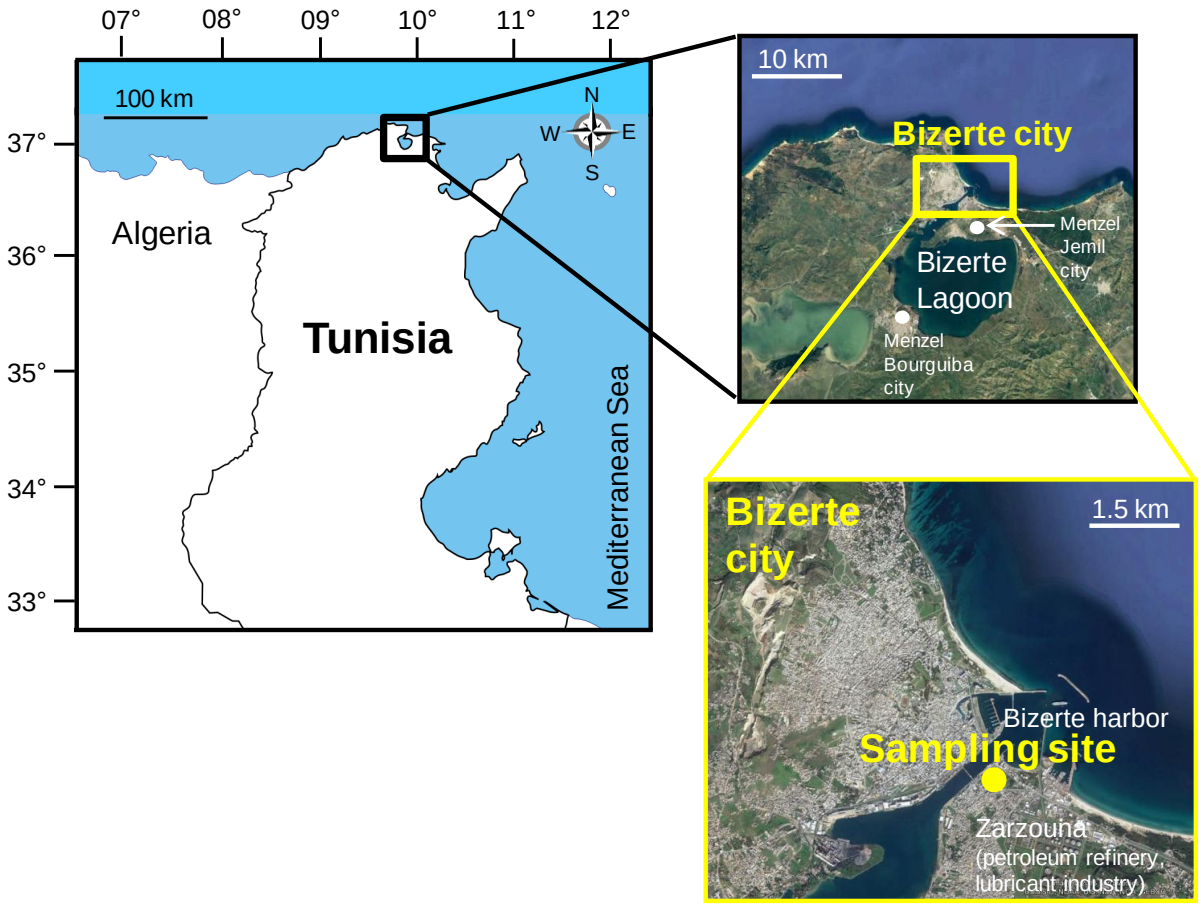

Figure S1. Location of the sampling site in Bizerte city (Tunisia, North Africa) (Barhoumi et al., 2018).

Table S1. Sampling details and meteorological data during the study period (March 2015–January 2016).

Month	Sampling period	Sampling duration (h)	Volume (m^3)	TSP ($\mu g\ m^{-3}$)	U ($m\ s^{-1}$)	WD	RH (%)	AT (°C)	P (mm)
Mar-15	02-04/03/15	48	1888.67	50.78	2.8	NW	76	18	0.0
Mar-15	04-06/03/15	48	1872.48	106.03	3.9	NW	75	14	4.7
Mar-15	11-13/03/15	48	1868.54	99.74	3.3	NW	77	11	0.0
Mar-15	13-15/03/15	48	1872.36	77.79	3.1	NNW	73	12	0.0
Mar-15	18-20/03/15	48	1879.90	44.36	6.1	NE	81	14	0.0
Mar-15	25-27/03/15	48	1905.13	49.77	6.4	NW	81	14	1.0
Mar-15	27-29/03/15	48	1888.65	71.34	10.3	WNW	75	14	0.0
Apr-15	07-09/04/15	48	1854.38	46.71	5.8	NNE	58	11	0.3
Apr-15	09-11/04/15	48	1883.44	40.71	3.9	NNE	68	14	0.0
Apr-15	17-19/04/15	48	1913.42	88.42	3.6	WSW	71	18	0.0
Apr-15	21-23/04/15	48	1894.08	45.70	3.6	SW	71	17	0.0
May-15	07-09/05/15	48	1927.44	111.52	5.6	WNW	67	21	0.0
May-15	12-14/05/15	48	1912.32	35.31	2.8	NNE	60	20	0.0
May-15	14-16/05/15	48	1943.55	81.70	3.6	NW	59	21	0.3
May-15	19-21/05/15	48	1936.98	88.55	4.2	NW	70	20	0.7
May-15	26-28/05/15	48	1912.60	75.19	7.2	NW	73	18	1.0
May-15	28-30/05/15	48	1926.39	37.64	4.4	SW	61	20	0.0
Jun-15	02-04/06/15	48	1917.50	48.91	3.3	NNW	71	20	0.0
Jun-15	09-11/06/15	48	1949.13	42.82	5.3	SE	67	25	0.0
Jun-15	11-13/06/15	48	1967.08	92.43	6.7	SE	58	27	0.0
Jun-15	18-20/06/15	48	1939.76	95.91	7.8	NW	70	22	0.0
Jun-15	24-26/06/15	48	1944.57	16.32	3.6	NNW	68	24	0.3
Jun-15	26-28/06/15	48	1943.92	43.94	5.8	NNW	67	24	0.0
Jul-15	03-05/07/15	48	1942.73	9.63	3.1	NNE	71	25	0.0
Jul-15	05-07/07/15	48	1956.95	38.70	3.3	SE	56	28	0.0
Jul-15	10-12/07/15	48	1954.09	41.23	3.9	NW	71	25	0.0
Jul-15	12-14/07/15	48	1962.44	89.41	6.4	NW	67	27	0.0
Jul-15	25-27/07/15	48	1973.14	50.80	3.6	NW	63	27	0.0
Jul-15	29-31/07/15	48	1995.17	58.48	2.2	NW	55	30	0.0
Aug-15	04-06/08/15	48	1973.60	47.29	1.9	NNW	64	28	0.0
Aug-15	07-09/08/15	48	1975.97	34.37	1.7	NNW	68	28	0.0
Aug-15	11-13/08/15	48	1964.42	25.85	5.8	NNW	67	27	0.3
Aug-15	13-15/08/15	48	1973.31	70.33	2.2	W	75	26	0.0
Aug-15	19-21/08/15	48	1951.85	60.67	4.4	NW	63	26	0.0
Aug-15	21-23/08/15	48	1956.63	30.98	2.8	NNW	67	26	0.0
Aug-15	27-29/08/15	48	1965.70	68.17	5.8	SE	68	29	0.0
Sep-15	02-04/09/15	48	1973.14	105.67	1.9	SE	65	27	0.3
Sep-15	05-07/09/15	48	1996.96	44.93	3.9	NW	63	25	0.3
Sep-15	11-13/09/15	48	1967.20	78.01	5.0	SW	63	28	0.0
Sep-15	16-18/09/15	48	1989.74	119.06	4.7	SW	56	29	0.0
Oct-15	16-18/10/15	48	1935.82	57.69	1.9	SW	67	21	0.0
Oct-15	22-24/10/15	48	1909.94	64.10	5.6	NNE	67	17	1.0
Oct-15	27-29/10/15	48	1921.69	41.94	2.8	NW	79	20	0.0
Nov-15	04-06/11/15	48	1908.41	56.28	2.8	NW	84	19	0.0
Nov-15	11-13/11/15	48	1893.83	65.30	1.4	NW	84	17	0.0
Nov-15	20-22/11/15	48	1914.44	99.46	7.5	NW	66	18	0.0
Nov-15	27-29/11/15	48	1879.78	37.71	7.2	NW	71	14	2.0
Dec-15	04-06/12/15	48	1857.30	83.53	1.1	ESE	78	15	0.0
Dec-15	18-21/12/15	48	1853.05	64.44	0.8	NE	85	12	0.0
Dec-15	23-25/12/15	48	1852.71	54.24	1.9	SW	84	12	0.0
Jan-16	13-15/01/16	48	1866.33	58.06	3.1	WNW	76	12	0.7
Jan-16	27-29/01/16	48	1840.11	50.24	3.9	SSW	82	14	0.0
Jan-16	29-31/01/16	48	1863.08	86.22	6.9	NW	63	13	0.0

TSP total suspended particles, *U* wind speed, *WD* wind direction, *RH* relative humidity, *AT* ambient temperature, *P* precipitation.
Meteorological data from Bizerte city were provided by the National Institute of Meteorology.

Table S2. Method detection limits (MDLs) of PAHs and AHs in the gas phase (pg m^{-3}).

PAHs		AHs	
Nap	0.3	C_{15}	3
Acy	0.3	C_{16}	3
Ace	0.3	C_{17}	3
Fl	0.3	C_{18}	3
DBT	0.3	C_{19}	3
Phe	0.3	C_{20}	5
Ant	0.3	C_{21}	5
Flu	0.3	C_{22}	5
Pyr	0.3	C_{23}	5
BaA	3	C_{24}	5
Chr	3	C_{25}	5
BbF	3	C_{26}	5
BkF	3	C_{27}	5
BeP	3	C_{28}	5
BaP	3	C_{29}	5
Per	3	C_{30}	5
DahA	3	C_{31}	10
IcdP	3	C_{32}	10
BghiP	3	C_{33}	10
C1-Nap	0.3	C_{34}	10
C2-Nap	0.3	C_{35}	10
C3-Nap	0.3	C_{36}	10
C1-Fl	0.3	C_{37}	10
C2-Fl	0.3	C_{38}	10
C3-Fl	0.3	C_{39}	10
C1-Phe	0.3	C_{40}	10
C2-Phe	0.3	Pr	3
C3-Phe	0.3	Phy	3
C1-Pyr	0.3		
C2-Pyr	0.3		
C3-Pyr	3		
C1-Chr	3		
C2-Chr	3		
C3-Chr	3		

Table S3. Parameters used for temperature correction of subcooled liquid vapour pressure ($P_L^{0,*}$) and octanol-air partition coefficient (K_{OA}).

Compounds	$\log(P_L^0, \text{Pa}) = m_L/T + b_L$		$P_L^0 = P_L^{0,*} * \exp(\frac{\triangle H_{vap}^0}{R}(\frac{1}{298.15} - \frac{1}{T}))$		$\text{Log } K_{OA} = A + B/T$	
	m_L	b_L	$\triangle H_{vap}^0(\text{kJmol}^{-1})$	$P_L^{0,*}(Pa)$	A	B
PAHs						
Nap	-3225[a]	12.66[a]			-3.954[a]	2960[a]
Acy	-3994[a]	14.15[a]			-5.443[a]	3729[a]
Fl	-3492[b]	11.43[b]			2.586[c]	1097[c]
DBT			78	2.7E-02	2.870[c]	1160[c]
Phe	-3675[a]	11.42[a]			-2.252[a]	2952[a]
Ant	-3703[a]	11.47[a]			-2.300[a]	2980[a]
Flu	-4298[a]	12.45[a]			-3.279[a]	3575[a]
Pyr	-4164[b]	11.7[b]			3.446[c]	1170[c]
BaA	-5217[a]	13.93[a]			-4.758[a]	4493[a]
Chr	-5228[a]	13.94[a]			-4.773[a]	4505[a]
BbF	-5819[a]	14.82[a]			-5.651[a]	5096[a]
BkF	-5849[a]	14.87[a]			-5.703[a]	5126[a]
BeP	-5926[a]	14.96[a]			-5.792[a]	5203[a]
BaP	-5944[a]	14.98[a]			-5.815[a]	5220[a]
BghiP	-6443[a]	15.62[a]			-6.450[a]	5720[a]
AHs						
C17			86	3.0E-02		
Pr			87	5.8E-02		
C18			91	2.0E-02		
Phy			92	1.9E-02		
C19			96	6.5E-03		
C20			101	6.2E-03		
C21			107	4.2E-03		
C22			115	3.2E-03		
C23			120	1.2E-03		
C24			124	4.7E-04		
C25			129	1.7E-04		
C26			130	6.6E-05		
C27			137	2.5E-05		
C28			142	9.4E-06		
C29			146	3.5E-06		
C30			151	1.3E-06		
C31			155	5.0E-07		
C32			160	1.9E-07		
C33			164	7.1E-08		
C34			169	2.6E-08		
C35			173	1.0E-08		

[a] the values were acquired from Vuong et al. (2022); [b] the values were acquired from Lei et al. (2002); [c] the values were acquired from Parnis et al. (2015); the values for $\triangle H_{vap}^0$ (Enthalpy of vaporization at standard conditions (kJ mol^{-1})) were acquired from *https://www.chemeo.com/*, and the subcooled liquid vapor pressures ($P_L^{0,*}$) at 298.15 K were acquired from EPI Suite version 4.11 from the US EPA website (*http://www.epa.gov/opptintr/exposure/pubs/episuitedl.htm*).

Table S4. Toxic equivalent factors (TEF) of PAHs.

Compound	TEF	References
Nap [a]	0.001	Nisbet and LaGoy (1992)
Acy [a]	0.001	Nisbet and LaGoy (1992)
Ace [a]	0.001	Nisbet and LaGoy (1992)
Fl [a]	0.001	Nisbet and LaGoy (1992)
Phe [a]	0.001	Nisbet and LaGoy (1992)
Ant [a]	0.01	Nisbet and LaGoy (1992)
Flu [a]	0.001	Nisbet and LaGoy (1992)
Pyr [a]	0.001	Nisbet and LaGoy (1992)
BaA [a]	0.1	Nisbet and LaGoy (1992)
Chr [a]	0.01	Nisbet and LaGoy (1992)
BbF [a]	0.1	Nisbet and LaGoy (1992)
BkF [a]	0.1	Nisbet and LaGoy (1992)
BeP	0.01	Hsu et al. (2014)
BaP [a]	1	Nisbet and LaGoy (1992)
Per	0.001	Hsu et al. (2014)
DahA [a]	1	Nisbet and LaGoy (1992)
IcdP [a]	0.1	Nisbet and LaGoy (1992)
BghiP [a]	0.01	Nisbet and LaGoy (1992)
C1-Nap	0.0025	Durant et al. (1996)
C2-Nap	0.001	Nisbet and LaGoy (1992)
C1-Phe	0.001	CalEPA (2020)
C1-Pyr	0.1	CalEPA (2020)

[a] EPA priority PAHs

Table S5. Parameters used in the incremental lifetime cancer risk (ILCR) assessment for the different age groups.

Exposure parameter	Unit	Distribution	Infants	Children	Adolescents	Adults
			0-1 year	1-11 years	12-17 years	18-70 years
Inhalation rate ($IR_{inhalation}$)[a]	m^3 day^{-1}	Normal	5.96 ± 1.49	14.10 ± 1.72	32.13 ± 1.04	32.73 ± 1.14
BaP-TEQ–gas+particle (22 PAHs)	ng m^{-3}	Log-normal	0.25 ± 0.31	0.25 ± 0.31	0.25 ± 0.31	0.25 ± 0.31
Exposure frequency (EF)[b]	days $year^{-1}$	Uniform	252 ± 1.01	252 ± 1.01	252 ± 1.01	252 ± 1.01
Exposure duration (ED)[c]	years	Uniform	1	11	6	52
Body weight (BW)[d]	kg	Normal	6.79 ± 1.27	16.68 ± 1.48	32.41 ± 1.08	59.78 ± 1.07
Average life span (ALT)[e]	years	Uniform	70	70	70	70
Cancer slope factor ($CSF_{inhalation}$)[f]	(mg kg^{-1} day^{-1})$^{-1}$	Uniform	3.14 ± 1.80	3.14 ± 1.80	3.14 ± 1.80	3.14 ± 1.80

[a] Adopted from ICPR, 1994.

[b] Adopted from Central Personnel Administration, ROC (*http://www.cpa.gov.tw/cpa2004/pfattend/download/EXWT93102901.doc*).

[c] Adopted from Yang et al. (2014).

[d] Adopted from department of Health, ROC (*http://www.doh.gov.tw/cht/index.aspx#)*,Chen et al. (2012) and Wu et al. (2011).

[e] Adopted from Lu et al. (2016).

[f] Adopted from Chen and Liao, 2006.

Table S6. Statistical summary of K_p x TSP and log K_p for each PAH and AH congener.

Compound	K_p x TSP					Compound	log K_p				
	n	Mean	Min	Median	Max		*n*	Mean	Min	Median	Max
PAHs						**PAHs**					
Nap	27	0.493	0.030	0.158	4.231	Nap	27	-2.506	-3.515	-2.533	-1.153
Acy	44	0.205	0.002	0.081	3.256	Acy	44	-2.950	-4.379	-2.934	-1.248
Fl	53	0.072	0.002	0.049	0.513	Fl	53	-3.092	-4.600	-3.074	-1.964
DBT	36	0.026	0.001	0.014	0.140	DBT	36	-3.625	-4.620	-3.658	-2.748
Phe	53	0.022	0.001	0.018	0.127	Phe	53	-3.550	-4.841	-3.530	-2.572
Ant	48	0.061	0.002	0.025	0.488	Ant	48	-3.251	-4.737	-3.373	-1.987
Flu	53	0.083	0.001	0.054	0.609	Flu	53	-3.195	-9.204	-3.029	-1.950
Pyr	53	0.096	0.001	0.065	0.779	Pyr	53	-3.129	-9.061	-2.993	-1.843
BaA	47	1.877	0.074	0.847	8.024	BaA	47	-1.747	-3.088	-1.869	-0.812
Chr	52	1.553	0.045	0.917	12.83	Chr	52	-1.803	-3.372	-1.898	-0.561
BbF	46	29.90	4.950	20.41	186.1	BbF	46	-0.456	-1.072	-0.553	0.427
BkF	27	14.51	1.737	9.426	47.80	BkF	27	-0.778	-1.542	-0.832	-0.072
BeP	41	26.98	0.823	22.89	85.48	BeP	41	-0.448	-1.997	-0.375	0.094
BaP	27	17.27	0.468	14.07	61.93	BaP	27	-0.816	-2.222	-0.705	-0.017
BghiP	27	62.10	13.91	55.53	122.9	BghiP	27	-0.042	-0.504	-0.043	0.355
Σ_{15}PAHs		91.51	0.562	66.94	369.4	Σ_{15}PAHs		-26.78	-36.52	-27.50	-13.46
AHs						**AHs**					
C_{17}	44	0.986	0.005	0.445	7.524	C_{17}	44	-2.146	-4.230	-2.116	-0.808
C_{18}	48	0.114	0.004	0.089	0.430	C_{18}	48	-2.872	-3.989	-2.842	-1.849
C_{19}	53	0.065	0.006	0.062	0.190	C_{19}	53	-3.023	-3.912	-2.947	-2.306
C_{20}	53	0.059	0.006	0.050	0.254	C_{20}	53	-3.064	-4.134	-3.062	-2.289
C_{21}	53	0.094	0.012	0.059	0.407	C_{21}	53	-2.911	-3.884	-3.002	-2.125
C_{22}	53	0.187	0.019	0.119	1.045	C_{22}	53	-2.637	-3.661	-2.631	-1.687
C_{23}	53	0.404	0.032	0.252	1.843	C_{23}	53	-2.354	-3.156	-2.360	-1.499
C_{24}	53	1.107	0.059	0.697	4.978	C_{24}	53	-1.950	-2.805	-1.943	-1.082
C_{25}	53	3.442	0.208	2.085	15.30	C_{25}	53	-1.442	-2.285	-1.418	-0.609
C_{26}	53	7.362	0.394	4.025	37.01	C_{26}	53	-1.162	-2.061	-1.222	-0.192
C_{27}	53	19.36	0.739	9.664	332.3	C_{27}	53	-0.782	-1.985	-0.742	0.821
C_{28}	52	20.85	0.423	13.75	108.3	C_{28}	52	-0.681	-2.226	-0.629	0.489
C_{29}	53	40.54	0.945	38.83	123.8	C_{29}	53	-0.309	-1.878	-0.219	0.917
C_{30}	52	54.47	0.376	35.90	381.8	C_{30}	52	-0.305	-2.278	-0.201	1.005
C_{31}	53	29.29	1.528	22.64	113.3	C_{31}	53	-0.480	-1.602	-0.450	0.513
C_{32}	45	21.21	0.787	19.23	97.73	C_{32}	45	-0.647	-2.051	-0.498	0.306
C_{33}	46	28.05	2.858	20.96	143.0	C_{33}	46	-0.473	-1.436	-0.358	0.434
C_{34}	31	21.61	2.214	14.90	180.5	C_{34}	31	-0.657	-1.578	-0.618	0.447
C_{35}	27	25.87	3.088	20.86	91.82	C_{35}	27	-0.574	-1.446	-0.583	0.415
Pr	37	1.474	0.069	0.841	8.024	Pr	37	-1.831	-2.898	-1.917	-0.763
Phy	40	0.366	0.014	0.248	1.117	Phy	40	-2.372	-3.745	-2.315	-1.235
Σ_{21}AHs		238.2	23.38	210.9	634.8	Σ_{21}AHs		-30.10	-47.32	-29.85	-15.26

n: number of data points. Only those PAHs and AHs having concentrations above the MDLs in both the gas and particle phases for a given sample/event have been considered.

Table S7. Comparison of log K_p *versus* log P_L^0 regressions for PAHs and AHs at various locations worldwide.

Sampling area	n	m_r	b_r	R^2	Reference
PAHs					
Bizerte city, Tunisia	53	-0.71 (-0.95 to -0.32)	-4.40 (-5.94 to -2.93)	0.85 (0.60 to 1.00)	This study
Four climate zones, China	26	-0.65 to -0.47	-4.84 to -3.93	0.93 to 0.80	Wei et al. (2021)
Lhasa, China	18	-0.50 (-0.66 to -0.31)	-3.96 (-4.54 to -3.64)	0.51 to 0.90	Gong et al. (2011)
Agra, India	40	-2.83 to -0.04	-6.68 to -2.54	0.58 to 0.98	Verma et al. (2017)
Ovaakca and Cumalikizik, Turkey	52-72	-0.505 to -0.319	-3.535 to -3.166	0.455 to 0.652	Ayyildiz and Esen (2020)
Eskişehir, Turkey	60	-0.334 to -0.314	-3.245 to -2.962	0.59 to 0.60	Gaga and Arı (2019)
Zonguldak, Turkey	84	-0.49 (-0.63 to -0.29)	-4.70 (-5.60 to -3.78)	0.88 (0.64 to 0.96)	Akyüz and Çabuk (2010)
Zaragoza, Spain	48	-1.20 to -0.17	-5.22 to -1.76	0.74 to 1.00	Callen et al. (2008)
Prato, Italy	11	-0.81 to -0.64	-7.06 to -5.68	0.87 to 0.98	Cincinelli et al. (2007)
Heraklion, Greece	16	-1.01 to -0.69	-7.77 to -6.19	0.94 to 0.99	Tsapakis and Stephanou (2005)
Athens, Greece	19	-1.49 to -0.16	-6.50 to -2.80	0.47 to 0.93	Sitaras et al. (2004)
AHs					
Bizerte city, Tunisia	53	-0.46 (-0.98 to -0.28)	-3.59 (-5.48 to -2.67)	0.78 (0.53 to 0.96)	This study
Prato, Italy	11	-0.84 to -0.32	-8.53 to -5.07	0.74 to 0.99	Cincinelli et al. (2007)
Athens, Greece	8	-0.57 to -0.25	-5.24 to -4.22	0.47 to 0.99	Mandalakis et al. (2002)

n: number of data points.

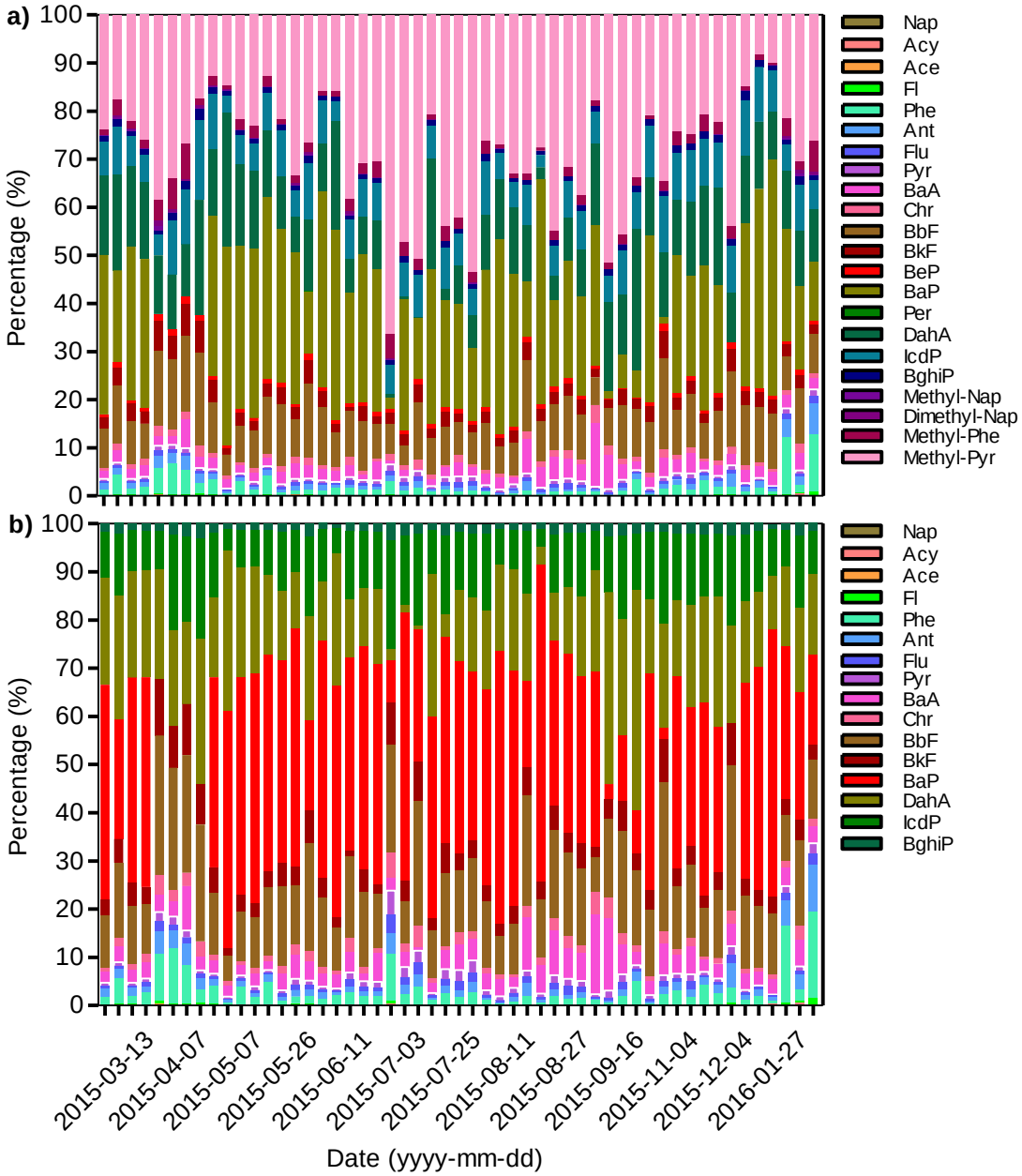

Figure S2. Percentage contributions of individual PAHs to the total BaP-TEQ of Σ_{22}PAHs (**a**) and Σ_{16}USEPA-PAHs (**b**).

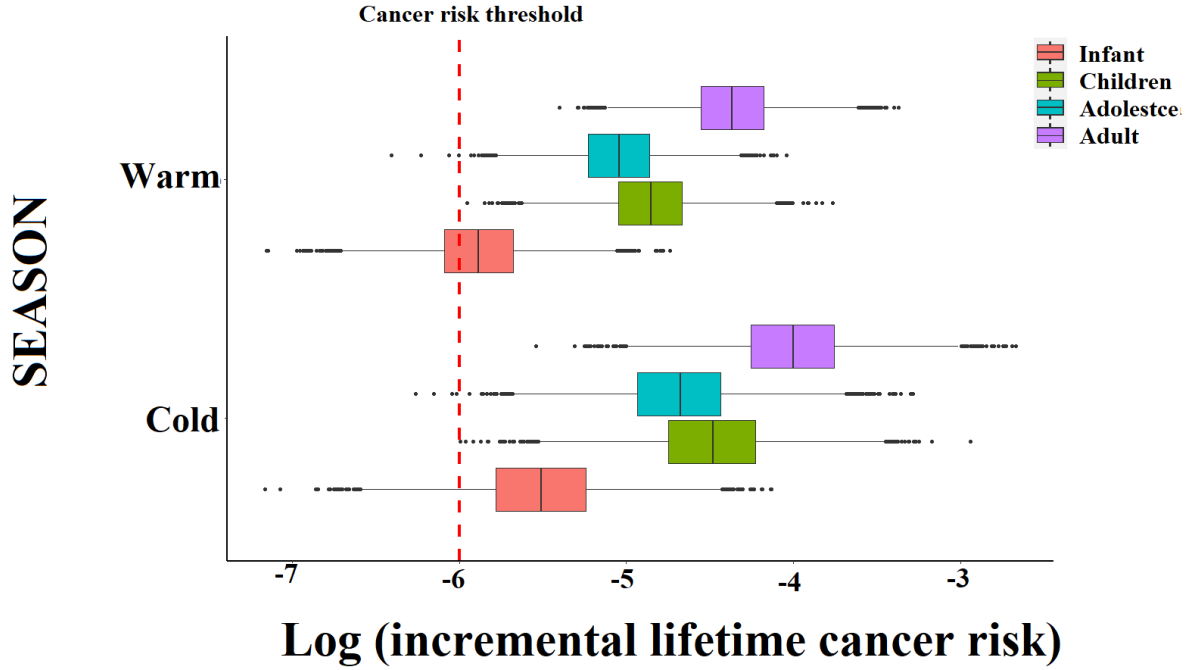

Figure S3. Boxplot of incremental lifetime cancer risk (ILCR) associated with exposure to PAHs present in both gas and particle phases of outdoor air in Bizerte city for the period from March 2015 to January 2016, and grouped by season and age.

References

Akyüz, M., Çabuk, H., 2010. Gas–particle partitioning and seasonal variation of polycyclic aromatic hydrocarbons in the atmosphere of Zonguldak, Turkey. Sci. Total Environ. 408, 5550–5558.

Ayyildiz, E.G., Esen, F., 2020. Atmospheric Polycyclic Aromatic Hydrocarbons (PAHs) at Two Sites, in Bursa, Turkey: Determination of Concentrations, Gas–Particle Partitioning, Sources, and Health Risk. Arch. Environ. Contam. Toxicol. 78, 350–366.

Barhoumi, B., Castro-Jiménez, J., Guigue, C., Goutx, M., Sempéré, R., Derouiche, A., Achour, A., Touil, S., Driss, M.R., Tedetti, M., 2018. Levels and risk assessment of hydrocarbons and organochlorines in aerosols from a North African coastal city (Bizerte, Tunisia). Environ. Pollut. 240, 422–431.

CalEPA, 2020. California State Environmental Protection Agency. Office of Environmental Health Hazard Assessment. Available at *https://oehha.ca.gov/chemicals/*.

Callen, M.S., Cruz, M.T., Lopez, J.M., Murillo, R., Navarro, M.V., Mastral, A.M., 2008. Some inferences on the mechanism of atmospheric gas/particle partitioning of polycyclic aromatic hydrocarbons (PAH) at Zaragoza (Spain). Chemosphere 73, 1357–1365.

Chen, J.W., Wang, S.L., Hsieh, D.P.H., Yang, H.H., Lee, H.L., 2012. Carcinogenic potencies of polycyclic aromatic hydrocarbons for back-door neighbors of restaurants with cooking emissions. Sci. Total Environ. 417–418, 68–75.

Chen, S., Liao, C., 2006. Health risk assessment on human exposed to environmental polycyclic aromatic hydrocarbons pollution sources. Sci. Total Environ. 366, 112–123.

Cincinelli, A., Del Bubba, M., Martellini, T., Gambaro, A., Lepri, L., 2007. Gas-particle concentration and distribution of n-alkanes and polycyclic aromatic hydrocarbons in the atmosphere of Prato (Italy). Chemosphere 68, 472–478.

Durant, J.L., Busby, Jr.W.F., Lafleur, A.L., Penman, B.W., Crespi, C.L., 1996. Human cell mutagenicity of oxygenated, nitrated and unsubstituted polycyclic aromatic hydrocarbons associated with urban aerosols. Mutat. Res. 371, 123–157.

Gaga, E.O., Arı, A., 2019. Gas-particle partitioning and health risk estimation of polycyclic aromatic hydrocarbons (PAHs) at urban, suburban and tunnel atmospheres: Use of measured EC and OC in model calculations. Atmos. Pollut. Res. 10, 1–11.

Gong, P., Wang, X., Yao, T., 2011. Ambient distribution of particulate- and gas-phase n-alkanes and polycyclic aromatic hydrocarbons in the Tibetan Plate. Environ. Earth Sci. 64, 1703–1711.

Hsu, H.-I., Lin, M.-Y., Chen, Y.-C., Chen, W.-Y., Yoon, C., Chen, M.-R., Tsai, P.-J., 2014. An Integrated Approach to Assess Exposure and Health-Risk from Polycyclic Aromatic Hydrocarbons (PAHs) in a Fastener Manufacturing Industry. Int. J. Environ. Res. Public Health 11, 9578–9594.

ICRP, 1994. Human Respiratory Tract Model for Radiological Protection. ICRP Publication, Elsevier, New York, NY.

Lei, Y.D., Chankalal, R., Chan, A., Wania, F., 2002. Supercooled Liquid Vapor Pressures of the Polycyclic Aromatic Hydrocarbons, J. Chem. Eng. Data 47, 801–806.

Mandalakis, M., Tsapakis, M., Tsoga, A., Stephanou, E.G., 2002. Gas–particle concentrations and distribution of aliphatic hydrocarbons, PAHs, PCBs and PCDD/Fs in the atmosphere of Athens (Greece). Atmos. Environ. 36, 4023–4035.

Nisbet, I.C.T., LaGoy, P.K., 1992. Toxic equivalency factors (TEFs) for polycyclic aromatic hydrocarbons (PAHs). Regul. Toxicol. Pharmacol. 16, 290–300.

Parnis, J.M., Mackay, D., Harner, T., 2015. Temperature dependence of Henry's law constants and KOA for simple and heteroatom-substituted PAHs by COSMO-RS. Atmos. Environ. 110, 27–35.

Sitaras, I.E., Bakeas, E.B., Siskos, P.A., 2004. Gas/particle partitioning of seven volatile polycyclic aromatic hydrocarbons in a heavy traffic urban area. Sci. Total Environ. 327, 249–264.

Tsapakis, M., Stephanou, E.G., 2005. Occurrence of gaseous and particulate polycyclic aromatic hydrocarbons in the urban atmosphere: study of sources and ambient temperature effect on the gas/particle concentration and distribution. Environ. Pollut. 133, 147–156.

Verma, P.K., Sah, D., Kumari, K.M., Lakhani, A., 2017. Atmospheric concentrations and gas–particle partitioning of polycyclic aromatic hydrocarbons (PAHs) and nitro-PAHs at Indo-Gangetic sites. Environ. Sci.: Processes Impacts 19, 1051–1060.

Vuong, Q.T., Son, J.-M., Thang, P.Q., Ohura, T., Choi, S.-D., 2022. Application of gas chromatographic retention times to determine physicochemical properties of nitrated, oxygenated, and parent polycyclic aromatic hydrocarbons. Environ. Pollut. 294, 118644.

Wei, C., Bandowe, B.A., Han, Y., Cao, J., Watson, J.G., Chow, J.C., Wilcke, W., 2021. Polycyclic aromatic compounds (PAHs, oxygenated PAHs, nitrated PAHs, and azaarenes) in air from four climate zones of China: Occurrence, gas/particle partitioning, and health risks. Sci. Total Environ. 786, 147234.

Wu, B., Zhang, Y., Zhang, X.X., Cheng, S.P., 2011. Health risk assessment of polycyclic aromatic hydrocarbons in the source water and drinking water of China: quantitative analysis based on published monitoring data. Sci. Total Environ. 410–411, 112–118.

Yang, W., Lang, Y., Li, G., 2014. Cancer risk of polycyclic aromatic hydrocarbons (PAHs) in the soils from Jiaozhou Bay wetland. Chemosphere 112, 289–295.

1